

WriteSAE: Sparse Autoencoders for Recurrent State

Jack Young
Indiana University
youngjh@iu.edu

Abstract

We introduce WriteSAE, a sparse autoencoder for the matrix updates written into recurrent language-model state. In Gated DeltaNet, Mamba-2, and RWKV-7, each token writes a matrix-shaped update to a recurrent cache; a residual-stream SAE has vector-shaped atoms and cannot replace that update directly. WriteSAE learns rank-1 matrix atoms with the same shape as the model’s own write. This lets us test a direct replacement: at positions where the SAE activates an atom, we remove the model’s write, insert the atom scaled by its SAE activation, and continue the forward pass. The atom gives a closer final token distribution than deleting the write on **92.4%** of evaluated positions; averaged per atom, the rate is 89.8%. For Gated DeltaNet, a formula using the forget gate, read query, and output embedding predicts the resulting logit change with $R^2=0.98$. The same replacement test transfers to Mamba-2-370M at 88.1%. In generation, the formula chooses a write direction; writing it into three consecutive cache positions at $3\times$ the norm of the model’s write makes tokens initially ranked 100–1000 by the unmodified model appear in **100%** of continuations, up from 33.3%. To our knowledge this is the first cache-level steering intervention reported in a state-space or hybrid recurrent layer.

1 Introduction

State-space and hybrid recurrent models (Mamba-2, RWKV-7, Gated DeltaNet, Qwen3.5) write memory into a matrix cache rather than only into the residual stream. In the GDN recurrence of Yang et al. [2025b], each token adds one rank-1 matrix $\mathbf{k}_t \mathbf{v}_t^\top$ to a $d_k \times d_v$ state; later tokens read that state with a query $\mathbf{q}_{t'}$. Across a long context, many updates share the same state, and superposition theory predicts overlap among the features carrying them [Elhage et al., 2022, Scherlis et al., 2022].

Residual SAEs [Bricken et al., 2023, Cunningham et al., 2024, Templeton et al., 2024, Gao et al., 2025] and Mamba/RWKV extensions [Wang et al., 2025, Paulo et al., 2024, Hossain et al., 2025, Sunku Mohan et al., 2026] analyze vectors produced by a layer. Here the object is the matrix state that later tokens read. A standard SAE can be trained on $\text{vec}(S_t)$, but its decoder atoms are $d_k d_v$ -vectors. Replacing one model update requires an outer product because the next layer reads the state with a query. Fast-weight work already casts the per-token update as rank-1 [Schmidhuber, 1992, Ba et al., 2016, Schlag et al., 2021]; WriteSAE uses the same shape for the dictionary.

WriteSAE decoder atoms are rank-1 matrices $\mathbf{v}_i \mathbf{w}_i^\top$ shaped like GDN’s $\mathbf{k}_t \mathbf{v}_t^\top$, so a single atom can replace one cache update while preserving the shape read downstream (Fig. 1). A *firing* is a token position where the SAE assigns a nonzero coefficient to an atom. The atoms split into two behaviors: some align tightly with a single native write at the positions where they fire; others spread their direction across many writes. Section 3.1 names these populations and reports the Gaussian-mixture fit.

Preprint.

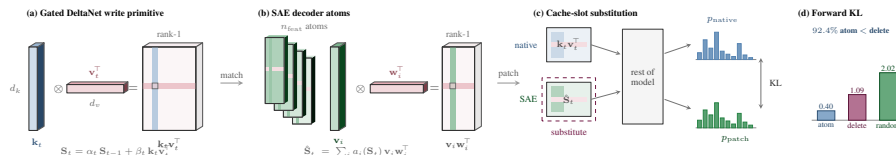


Figure 1: **WriteSAE atoms can replace native Gated DeltaNet writes.** At a primary GDN layer-head, atoms beat deleting the write on 92.4% of evaluated token positions; panels show the model write $\mathbf{k}_t \mathbf{v}_t^\top$, the learned atom $\mathbf{v}_i \mathbf{w}_i^\top$, the replacement test, and the KL controls.

Contributions.

- (1) A replacement test in which a learned rank-1 atom replaces the native Gated DeltaNet write; atoms beat deleting the write on 92.4% of evaluated positions (Section 3.2).
- (2) A formula for logit change, using the gate, read query, and output embedding, that predicts measured effects at median $R^2=0.98$ (Section 6.2).
- (3) Cache erasure and generation probes showing targeted logit and continuation changes where the formula is accurate (Section 4).
- (4) The same replacement test on Mamba-2-370M, where atoms beat deleting the write on 88.08% of evaluated positions (Section 3.3).

The replacement test runs at a single GDN layer-head: replace the native write with one learned atom scaled by its SAE coefficient, compare against deleting the write and against a random atom with the same coefficient, and measure KL divergence at the final output distribution. Atoms beat deleting the write on 92.4% of evaluated positions, and the per-atom average is 89.8% (Section 3.2). We also derive a formula for how one rank-1 perturbation changes a candidate token’s logit; it tracks measured effects at median $R^2=0.98$ (Section 6.2).

The same formula supplies directions for three cache interventions (Section 4). Erasing a single atom’s contribution on its firing positions drops the promoted token’s log probability by 0.116 nats. Single-position edits have the predicted sign on 84.6% of tested atom-token-context triples. During generation, writing the direction into three cache positions at $3\times$ makes tokens initially ranked 100–1000 by the unmodified model appear in **100%** of continuations, up from 33.3%, with +1.27 nats of first-step support.

Transfer depends on the model’s write rule. The same replacement test reaches 88.08% on Mamba-2-370M (Section 3.3). Across the tested recurrent families, the median cosine between an atom and the nearest native write at its firing positions is highest in GDN (0.262), then RWKV-7 (0.180), then Mamba-2 (0.0575). Four reported failures define the current scope: the larger Qwen model, the Mamba-2 closed-form logit shift, rank-2 atoms, and Mamba-2 generation edits. Code and checkpoints are at <https://github.com/JackYoung27/writesae>.

2 Method

For Gated DeltaNet, suppose we add a small rank-1 matrix $\varepsilon \mathbf{v}_i \mathbf{w}_i^\top$ to the cached state at position t_0 . We predict the resulting change in the logit of token tok at a later position t by

$$\Delta \ell_{\text{tok}}(c, i, t) \approx G_{t_0 \rightarrow t}(c) \langle \mathbf{w}_i, \mathbf{q}_t(c) \rangle \langle \mathbf{v}_i, W_U[\text{tok}] \rangle. \quad (1)$$

Here $\Delta \ell_{\text{tok}}(c, i, t)$ is the logit change in context c . Every quantity on the right is observable from a single forward pass. The scalar $G_{t_0 \rightarrow t}(c) = \prod_{s=t_0+1}^t \alpha_s(c)$ is the product of the model’s forget gates, \mathbf{q}_t is the query that reads the cache, and $W_U[\text{tok}]$ is the output-embedding row for the token. Section 3.2 compares this formula with measured logit changes and obtains population $R^2=0.98$.

Where the expression comes from. Gated DeltaNet writes one rank-1 outer $\mathbf{k}_t \mathbf{v}_t^\top$ into the matrix state S_t per token. The host recurrence is the gated delta rule of Yang et al. [2025b],

$$S_t = \alpha_t (I - \beta_t \mathbf{k}_t \mathbf{k}_t^\top) S_{t-1} + \beta_t \mathbf{k}_t \mathbf{v}_t^\top. \quad (2)$$

Subtracting perturbed and native trajectories cancels the additive write at every later step, leaving

$$\delta S_{s+1} = \alpha_{s+1}(c) (I - \beta_{s+1}(c) \mathbf{k}_{s+1}(c) \mathbf{k}_{s+1}(c)^\top) \delta S_s, \quad \delta S_{t_0} = \varepsilon \mathbf{v}_i \mathbf{w}_i^\top, \quad (3)$$

so later steps only multiply the perturbation by matrices the model already computes. When \mathbf{w}_i is nearly orthogonal to later keys, the extra term from $\mathbf{k}_{s+1} \mathbf{k}_{s+1}^\top$ is small; empirically this is the regime where the R^2 fit is high. Reading δS_t with the query \mathbf{q}_t and projecting to logits gives the two inner products in Eq. (1). App. A gives the full derivation.

Atom rank matches host write rank. A decoder atom with the same rank as the model’s update can replace one native rank-1 write while preserving the matrix shape. WriteSAE trains a TopK SAE whose decoder atoms factor as $\mathbf{v}_i \mathbf{w}_i^\top$ on mean-centered state $\mathbf{x} = \text{vec}(S_t - M)$ [Gao et al., 2025], minimizing $\|\mathbf{x} - \sum_{i \in \text{TopK}(\mathbf{a})} a_i \text{vec}(\mathbf{v}_i \mathbf{w}_i^\top)\|^2 + \lambda_{\text{aux}} \mathcal{L}_{\text{dead}}$, where $\text{TopK}(\mathbf{a})$ keeps the top- k entries of \mathbf{a} and $\mathcal{L}_{\text{dead}}$ revives inactive atoms. The loss is reconstruction MSE plus the auxiliary dead-feature loss; no norm-matching term is used during training. The rank-1 decoder costs $d_k + d_v = 256$ parameters per atom against $d_k d_v = 16,384$ for a FlatSAE dense atom (App. C). A flat atom can reconstruct the state but may mix several writes into one feature, making a single-write replacement test harder to interpret. We use WriteSAE for the rank-1 decoder matched to the model update;

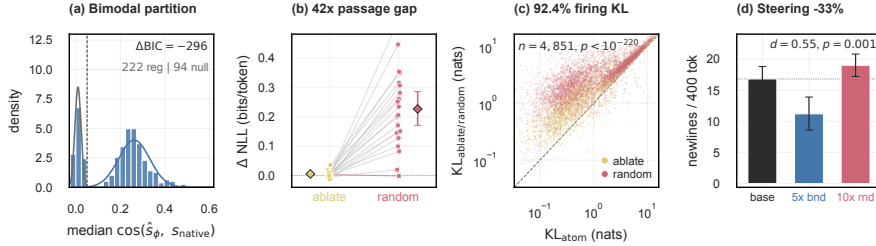


Figure 2: **Learned cache-write atoms produce lower KL at the final output distribution than deletion or random controls.** (a) Median cosine to the native write across the 316 alive atoms; a two-component GMM separates them into 222 registers and 94 bundles. (b) On 20 held-out OpenWebText passages, deleting every register firing costs +0.005 bits/token of passage NLL; a matched-norm random rank-1 write costs +0.226. (c) KL pooled across L1/L9/L17 evaluated positions, $n=4,851$, with the atom beating deletion on 92.4%. (d) Held-out Qwen3.5-4B generation probe: amplifying features more active at sentence boundaries reduces newlines from 16.8 to 11.2 ($p=0.001$, $d=0.55$).

BilinearSAE denotes the matched-filter encoder variant used in the 4B generation probe. The training corpus is 5,000 OpenWebText [Gokaslan and Cohen, 2019] sequences of length 1,024 run through Qwen3.5-0.8B [Yang et al., 2025a] at layers 1, 9, and 17, with an 80/20 split. Atoms whose decoded direction matches a native rank-1 write are *registers*; the rest are *bundles*. Section 3.2 validates this observational partition by GMM, class-swap controls, and seed-stable counts.

Replacement protocol. At firing (t, ℓ, h) , let $i^* = \arg \max_i a_i(t)$ be the atom with the largest TopK coefficient. The replacement protocol swaps the native write $\Delta_{\text{nat}} = \beta_t \mathbf{k}_t \mathbf{v}_t^\top$ for $\Delta_{\text{atom}} = a_{i^*}(t) \mathbf{v}_{i^*} \mathbf{w}_{i^*}^\top$, updates $S_t^{\ell, h} \mapsto S_t^{\ell, h} - \Delta_{\text{nat}} + \Delta_{\text{atom}}$, and continues the forward pass. The score is $\text{KL}(p_{\text{patched}} \| p_{\text{baseline}})$ on the final output distribution, the metric Zhang and Nanda [2024] recommend over logit-diff or accuracy for local activation patches.

3 Experiments

We test three claims: the learned atoms split into two observable classes, individual atoms can replace model writes, and replacement works best when the atom rank matches the model’s write rank. The causal metric is KL divergence between the final output distribution of the modified forward pass and the baseline.

Setup. We train WriteSAE on cached Gated DeltaNet states from Qwen3.5-0.8B. The training set is 5,000 OpenWebText [Gokaslan and Cohen, 2019] passages, sweeping layers $L \in \{1, 9, 17\}$ and heads $H \in \{0..15\}$. A cell is one (layer, head) pair. We use L9 H4 as the primary cell because a within-L9 sweep showed the largest separation between the two cosine components; the same ordering, atom better than deletion, then holds across the full layer (per-head distribution in Section 3.2). Cross-layer and cross-architecture extensions (DeltaNet, Mamba-2, GLA, Qwen3.5-4B/27B) follow in Section 3.3. The replacement test compares three conditions after one cache write: the SAE atom at its learned coefficient, deleting the write, and a random atom with the same coefficient. All KL values reported below are at the final output distribution. Partition statistics come from a two-component Gaussian mixture on median cosine with the native write. The full protocol is in App. J.

3.1 Feature classes

WriteSAE at Qwen3.5-0.8B L9 H4 trains 2,048 atoms; 316 survive on the validation split. A two-component Gaussian mixture on median cosine-to-native-write returns 222 registers (mean cosine 0.26) and 94 bundles against 1,732 null atoms, with Bayesian information criterion $\Delta\text{BIC} = -296$ over the one-component null (Figure 2a). Cosine is the only feature used for this partition. Class membership is descriptive: bundles substitute on 89.0% vs registers at 91.4% at population scale, Mann-Whitney $p=0.24$ (App. F.2). Here population scale means a per-atom substitution test over alive features, averaged across firing contexts. The causal probes in Section 3.2 evaluate the alive population on axes excluded from the partition. The bundle mode is not the dense-SAE-latents phenomenon of Sun et al. [2025]; App. I.3 gives the comparison.

Three checks keep the observational partition separate from the causal tests. A random rank-1 control leaves top- K overlap near 1 across 47/48 cells (Fig. 9), the logit-change formula predicts effects at $R^2=0.98$, and learned atoms beat deleting the write across alive atoms at 89.8% (App. F.2). Seed runs reproduce the partition at coefficient of variation 4–12% in counts and agree on $< 1\%$ of specific atoms at cosine > 0.9 [Paulo and Belrose, 2026]. Role counts are stable, but atom identities are seed-specific.

¹F758 has the highest cosine alignment (0.985) but fires at activation rate 5×10^{-4} , so its full context is in App. G.2.

Table 1: **Four seed-42 exemplar atoms used in the main text at Qwen3.5-0.8B L9 H4.** Activation rate orders the register rows; F1335 is the main register example because it fires on 5.24% of validation tokens. Per-atom IDs are seed-specific; cross-seed identity rate is $< 1\%$, while role classes reproduce. F87 is the bundle baseline in the native-norm control in Section 3.2.¹

Role exemplar (seed-42)	Role	Class	$\cos_v \uparrow$	$\cos_w \uparrow$	Fire rate	Top reader
F1335	delimiter gate	register	0.92	0.42	5.24%	L21 H10 at $7.5\times$
F63	factual-span register	register	0.88	0.63	2.69%	L17 H4 at $5.2\times$
F53	proper-noun register	register	0.99	0.74	0.09%	L5 H5 at $6.9\times$
F87	bundle control	bundle	0.02	0.01	15.9%	substitution inverts

Table 2: **Atom substitution gives the lowest median KL at the final output distribution in every layer; the atom beats deleting the write on more than 91% of positions per layer.** Each of the $n=4,851$ evaluated positions at Qwen3.5-0.8B head 4 contributes one triple of KL values: the atom at its firing coefficient, deleting the write, and a random atom scaled by the same coefficient. Cells report median \pm MAD/ \sqrt{n} ; row-winners are bold. The ratio summary is the ratio of the per-column medians.

Layer	n	$KL_{\text{atom}} \downarrow$	$KL_{\text{delete}} \downarrow$	$KL_{\text{random}} \downarrow$	atom wins
L1	1,500	2.07 ± 0.06	2.82 ± 0.07	3.58 ± 0.08	93.9%
L9	1,851	0.40 ± 0.02	1.09 ± 0.04	2.02 ± 0.05	91.2%
L17	1,500	1.82 ± 0.06	2.58 ± 0.07	3.43 ± 0.08	92.3%
<i>KL ratio (atom : deletion : random) = 1 : 2.70 : 4.90</i>					

Exemplars and the register role. Table 1 uses F1335, F63, and F53 because they fire on natural text and read into different downstream cells. F1335 fires at delimiters next to list numerals, F53 on BPE sub-pieces of just-introduced proper nouns, F63 on factual-span continuations (Fig. 11 in App. E shows top-firing snippets, intervention KL, and reader enrichment for each). Pairwise Jaccard at exact tokens averages 0.001 across the top ten registers, giving different surface triggers under similar write geometry. Independent seeds reproduce the partition at CV 4–12% in atom counts, with $< 1\%$ of specific atoms matching at cosine > 0.9 across seeds.

3.2 Mechanism validation

Substitution is a stronger criterion than reconstruction. The atom must replace the native write in the cache and preserve the downstream behavior. Across 20 held-out OpenWebText passages at L9 H4, deleting every register firing raises NLL by $+0.005$ bits/token, while matched-norm random rank-1 writes raise it by $+0.226$, a $41.87\times$ gap that holds in 19/20 passages (Figure 2b). The probes below ask whether the gap holds for single writes, across the two atom classes, and for logit changes predicted from the formula. Appendix G reports alternative-explanation controls.

Partition. The two-component split (Figure 2a) is observational at firing level: bundles substitute almost as well as registers at population scale (App. F.2), and matched-norm random-rank-1 selectivity holds at 0.9953 across 47/48 cells.² Substitution performance therefore belongs to the alive dictionary population as a whole, beyond the cosine partition.

Single-write replacement. At each firing we run three forward passes: the SAE atom $a_i(t) \cdot \mathbf{v}_i \mathbf{w}_i^\top$ replaces the native $\beta_t \mathbf{k}_t \mathbf{v}_t^\top$ write at position t , where i has the largest TopK coefficient; the deletion pass removes the write; the random pass draws a fresh atom and uses the same coefficient $a_i(t)$. The learned atom beats deleting the write on **92.4%** of $n=4,851$ firings, Wilson 95% CI [91.6, 93.1] (Fig. 3). Cluster-bootstrap by feature widens that to [90.91, 93.94].³ L1, L9, and L17 rates are 93.9%, 91.2%, and 92.3%, with Cliff’s $\delta = +0.825$ at L9 (paired Wilcoxon $p < 10^{-200}$). The strict chain $KL_{\text{atom}} < KL_{\text{delete}} < KL_{\text{random}}$ holds on 89.5% of firings, so atom direction matters beyond write removal. In the L9 H4 population test over 87 atoms, the atom beats deletion on 89.8% of firings on average, 95% CI [88.1, 91.3]. Bundle atoms ($n=57$) have mean 89.0% and register atoms ($n=30$) have mean 91.4%, a $+2.4\text{pp}$ gap that Mann-Whitney does not split at $p=0.24$. Replacement works for both cosine classes in the alive dictionary.

All L9 heads. The 92.4% result pools evaluated positions across L1/L9/L17 H4. To check head selection, we repeat the replacement test on every L9 head with firings (15/16; H12 is dead), giving a mean atom-beats-deletion rate of **89.3% \pm 2.6%**, range 82.6%–93.2%. L9 H4 sits at 90.8% on the L9-only pool, $+0.59\sigma$ above the L9 head mean. Per-head numbers and a strip plot are in App. F.1, Fig. 13.

²Null-cosine median 0.00136. $BIC(k=2) = -679.18$ and $BIC(k=3) = -683.33$; the marginal $\Delta BIC = -4.15$ is too small to change the two-component operational separator we report.

³5,000 resamples; the passage-clustered CI is [90.90, 93.39] over 164 clusters.

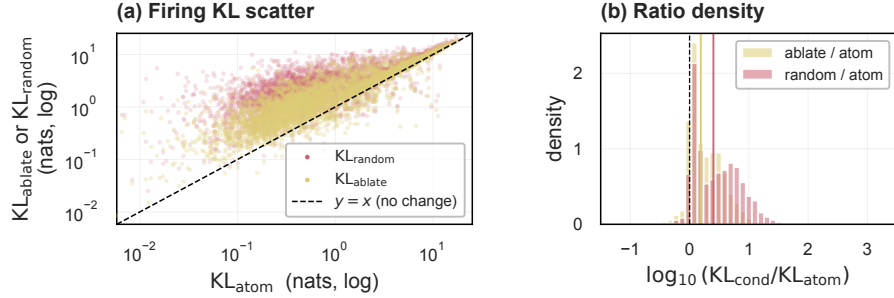


Figure 3: **Atom substitution beats both controls on 92.4% of $n=4,851$ evaluated positions at L1/L9/L17 H4.** Left: log-log scatter of KL_{delete} (red) and KL_{random} (green) against KL_{atom} , with $y=x$ for reference. Both distributions are above the identity line, and the strict chain $\text{atom} < \text{delete} < \text{random}$ holds on 89.5% of firings. Right: density of $\log_{10}(KL_{\text{cond}}/KL_{\text{atom}})$. The median ratio at each evaluated position is $1.55\times$ for deletion and $2.52\times$ for random, a $1.6\times$ separation of the controls; Table 2 reports the ratio of the per-column medians (1 : 2.70 : 4.90).

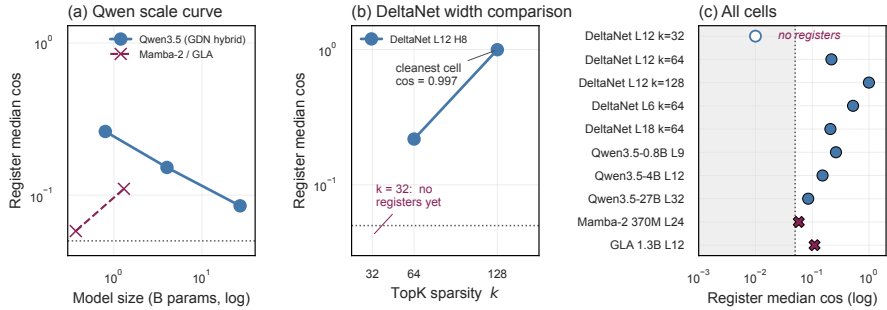


Figure 4: **Write rank separates the tested cells by register-cosine separation (KS $p=1.2 \times 10^{-10}$).** (a) Register median cosine down the Qwen3.5 ladder runs 0.262 (0.8B), 0.152 (4B), 0.085 (27B); Mamba-2 and GLA at matched scale stay below the 0.05 threshold. (b) DeltaNet L12 H8 over TopK sparsity: no register-class atoms at $k=32$, peak 0.997 at $k=128$. (c) All ten cells on a single log axis. Blue points are outer-product writes; red points are diagonal or scalar-gated states.

Logit-change formula. Per-feature median KL across alive register atoms is $4\text{--}7 \times 10^{-4}$, well below the random control.⁴ Pooled across firings the median is 0.40 (Table 2). The triple $KL_{\text{atom}} : KL_{\text{delete}} : KL_{\text{random}} = 1 : 2.70 : 4.90$ holds at L1 and L17. Eq. (1) predicts the logit change at one token from gates the model already computes, with no fitted parameters, and obtains median per-feature $R^2 = 0.98$ across seven registers and bundle F87 (App. A). The cosine factor accounts for the substitution gap; the output-embedding projection is not the limiting factor.

F87 fails when forced to native norm. F87 inverts when we amplify it to the native Frobenius norm. KL rises to $13\times$ the deletion condition, while register substitution at the same norm remains below the deletion floor.⁵ The two atoms differ only in their cosine to the native write. F87’s natural firing amplitude is small, so the population test cannot see the gap, and at natural amplitude F87 substitutes at 93.3%, indistinguishable from a register. The partition itself reappears at L1 ($\Delta\text{BIC} = -6,774$) and L17 (-390); across SAE seeds, counts move at CV 4–12% while $\approx 1\%$ of atoms reach cosine > 0.9 across seeds (orthogonal-control check in App. I.1).

Rank-2 decoder control. A rank-2 atom $A_i = \mathbf{v}_i^{(1)} \mathbf{w}_i^{(1)\top} + \mathbf{v}_i^{(2)} \mathbf{w}_i^{(2)\top}$ doubles parameters per entry. At all-16-head L9 substitution, rank-2 changes perplexity by $+0.82\%$ against $+0.76\%$ for rank-1, a $\Delta = +0.06\text{pp}$ parity result (App. F.3). Because Gated DeltaNet writes one rank-1 outer per step, rank-2 atoms do not improve the single-write replacement metric.

3.3 Architectural scope

Eq. (1) predicts that write rank, not parameter count, governs how closely atoms align with native writes. Five host architectures test the prediction. GDN and DeltaNet [Yang et al., 2024b] write rank-1 outers, RWKV-7 [Peng et al., 2025] writes rank-2, and Mamba-2 [Dao and Gu, 2024] and GLA [Yang et al., 2024a] update a diagonal state. Softmax attention is outside the scope; the variable here is the recurrent write rule. The partition appears across the $34\times$ Qwen3.5 scale range and a five-cell DeltaNet sparsity sweep (Figure 4).

⁴Top-1 match 1.00, per-feature KL 7–120 \times tighter than random; CV 6.5%/9.0% across seven registers and bundle F87. We deep-copy the cache per condition because Qwen3.5’s Gated DeltaNet mutates state in place.

⁵F87 at cosine 0.01: median KL 7.0×10^{-3} vs deletion 5.0×10^{-4} ; top-1 swap on 7% of firings.

DeltaNet and scale. DeltaNet L12 H8 at $k=128$ has the largest register/null separation we measured: register median cosine 0.997 and register/null ratio $383\times$. That cell runs with `use_gate=false`, so the update is purely bilinear in $\mathbf{k}_t \mathbf{v}_t^\top$; Qwen3.5 hybrids use the convex gate that DeltaNet drops. The Qwen3.5 cosine ladder reads 0.262 at 0.8B, 0.152 at 4B, and 0.085 at 27B (App. F, Fig. 12), with register counts of 220 and 147 at 4B and 27B. Qwen3.5-27B is $11.7\times$ below the DeltaNet cell even though both write rank-1 outers, consistent with the gate difference between them. Causal substitution at Qwen3.5-4B L12 H8 came out at chance under the same SAE recipe, a known training-objective gap (Section 6.2) rather than an architecture failure.

Host-matched WriteSAEs on Mamba-2 and RWKV-7. Each host architecture uses a WriteSAE decoder matching its native write rule.⁶ The observed register-cosine ordering is GDN (0.262) > RWKV-7 (0.180) > Mamba-2 (0.0575). Mamba-2-370M L24 H0 has 217 register atoms against 1,831 null; RWKV-7-1.5B L12 H0 has 200 register atoms against 541 null. The firing-level KS test uses cluster-bootstrap by feature with Holm correction over the four pairwise contrasts. GDN-Mamba-2 and DeltaNet-Mamba-2 clear $p_{\text{Holm}} < 10^{-6}$; the within-rank-1 DeltaNet-GDN comparison does not separate at $\alpha=0.05$, as expected when the only difference is gate strength. Cross-architecture crosscoders [Jiralerspong and Bricken, 2026] and feature universality [Lan et al., 2024] extend the write-rule question beyond residual-stream features.

Mamba-2 replacement test. At Mamba-2-370M L24 H0, we replace the native diagonal update $dt \cdot \text{diag}(\mathbf{B}_t) \cdot \mathbf{x}_t$ with a WriteSAE atom $a_i \cdot \mathbf{v}_i$, where \mathbf{v}_i is the SAE’s diagonal decoder atom and a_i is its activation. Atom beats deleting the write on **88.08%** of $n=2,500$ firings drawn from 100 atoms (60 register, 40 bundle by cosine partition), Wilson 95% CI [86.8, 89.3]. Median KL is 0.97 for the atom, 1.62 for deletion, and 2.32 for a random atom scaled by the same coefficient. The random control has $2.4\times$ higher KL than the atom; register and bundle are indistinguishable at Mann-Whitney $p=0.76$. Per-atom win rate is uncorrelated with cosine to the native write (Pearson $r=0.008$, $p=0.93$), matching the 0.8B GDN pattern. The averaged replacement test now succeeds in both GDN (89.8% at 87 atoms) and Mamba-2 (88.1% at 100 atoms). The 92.4% result is the single-write replacement rate at one GDN head; the cross-host ordering GDN > RWKV-7 > Mamba-2 supports the claim that the native write rule matters.

3.4 Ablations

Encoder and remaining ablations. At matched $n_f=2,048$, sparsity $k=32$, and training budget, WriteSAE’s bilinear encoder yields 32% dead features against FlatSAE’s 80% across a 720-run sweep (App. C), while BatchTopK and JumpReLU both recover the same register/bundle partition under the bilinear encoder (App. B). The encoder controls alive-feature count; the sparsity mechanism does not.

Probes, SVD, and SAE alternatives. Linear probes detect class membership but cannot substitute into the cache because the replacement must have the same rank-1 shape as the model write. PCA top-1 of writes is anti-correlated or near zero on every register exemplar (cosine -0.216 , -0.045 , -0.075 at F53, F63, F1335) while the SAE atom recovers the native write direction. The best-performing non-bilinear baseline in this sweep trains a flat TopK SAE on $\text{vec}(S_t)$ and substitutes its top-1 SVD outer product. On Mamba-2-370M L24 H0 the architecture-matched decoder improves over flat-SAE-SVD by $+6.55\text{pp}$ (82.85% vs 76.30%); on RWKV-7-1.5B L12 H0 both methods are near chance (45.3% vs 47.8%). On Qwen3.5-0.8B Gated DeltaNet L9 H4 the two finish within 0.11pp (91.25% vs 91.36%, $n=1,851$): gate decay already rank-1 dominates the state, so SVD top-1 of a flat-SAE atom recovers the direction the trained dictionary picks. The prior matters where the state is not rank-1 dominated by gating decay. Matching-pursuit SAE evaluation [Costa et al., 2025] reports similar host-agnostic ranking on transformer residuals; the substitution test here is architecture-aware.

4 Cache Intervention Probes

The closed-form expression of Section 6.2 explains a firing; it also chooses one. We use it as the engine for three interventions on a single GDN layer-head: erasing an atom on its own firings, writing the formula’s preferred direction at a single cache position, and writing that direction at three consecutive positions during decoding. A held-out 4B-scale probe then checks whether the same effects survive at scale. *Target inclusion* is our metric for the generation probes: the predicted token appears at least once in the 20-token greedy continuation.

⁶ $n_{\text{feat}}=2,048$. RWKV-7 register max cosine 0.671. GLA scalar-gated bilinear gives register median 0.110 [Yang et al., 2024a, Hu et al., 2025]. Residual atoms cannot occupy the cache slot (App. I.3).

Cache-slot erasure. Erasing one atom’s contribution affects only the token that atom promotes. Take F412 on Qwen3.5-0.8B L9 H4. At its $n=150$ natural firing positions, removing the rank-1 write from the cache drops the most-affected token’s log-probability by a median 0.116 nats (paired Wilcoxon $p=1.07 \times 10^{-6}$, 95% CI $[-0.265, -0.042]$). The same write at $n=150$ non-firing positions does not significantly change the logit (median $\Delta \log p=+0.016$ at $4 \times a^*$, $p=0.15$): context masks writes at positions where the atom would not have chosen to fire. Dose-response, target, and rank tables are in App. I.4.

Single-position sign prediction. For each target token T , the closed form picks a unit-norm direction $v_T^* = W_O[\text{head}]^\top W_U[T]/\|\cdot\|$ that should raise T ’s logit when written into the cache. Sign holds on 84.6% of $n=2,000$ trials (95% CI $[83.0, 86.2]$); magnitude is harder. Pearson correlation between predicted and measured shift comes out at $r=0.162$, with median measured-to-predicted ratio 1.08 and pooled $R^2=-0.06$. Small noisy effects swamp the pool. None of that matters for greedy decoding, because the target only has to overtake the native top-1 at one step. Per-feature breakdowns are in App. I.5.

Generation edit. One cache write often does not cross the bar. The target has to overtake the native top-1, and a single push can lose ground later. Three writes work better. Take tokens the unmodified model initially ranks between 100 and 1000 ($n=300$ contexts). Writing v_T^* at three consecutive cache positions with magnitude $m=3.0 \|\mathbf{k}_t \mathbf{v}_t^\top\|$ raises target inclusion from 33.3% to 100% under greedy decoding; the median rank shift is +517.

Pooled across the four target strata, the rate moves from 8.3% to 25.0% over 1,200 trials. Rank improves on 77.4% of trials. First-step logp lift is +1.27 nats (Table 3). Out-of-context targets shift rank but never reach top-1 inside 20 tokens.

The dose response is non-monotone. $m=1.5$ reaches 66.7% on mid-rank targets; $m=3.0$ reaches 100%; $m=6.0$ oversaturates back to 16.7% pooled. Full breakdown in App. I.6.

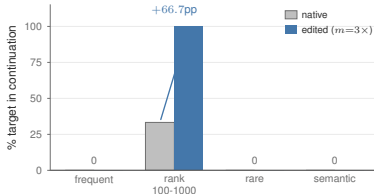


Figure 5: Writing the direction chosen by the formula at three cache positions raises target inclusion from 33.3% to 100% for targets initially ranked 100–1000 by the unmodified model ($n=300$). Target inclusion by class at $m=3 \times$ on Qwen3.5-0.8B L9 H4; native (gray) vs edited cache (atom-blue). Out-of-context targets shift rank but remain at 0%.

Table 3: Directions chosen by the formula increase target inclusion in a constrained generation probe. Pooled rows include frequent targets, targets initially ranked 100–1000 by the unmodified model, rare targets, and semantic targets at Qwen3.5-0.8B L9 H4 (Fig. 5; App. I.6).

Target set	n	target in continuation	native	first-step lift
Pooled	1,200	25.0%	8.3%	+1.27 nats
Ranks 100–1000	300	100%	33.3%	+1.27 nats

Newline-rate edit on a held-out 4B model. The same dictionary transfers to a larger host: Qwen3.5-4B-Base at layer 9, with no retraining. The boundary signal is concentrated. Score each feature by mean activation on sentence-boundary tokens minus mean activation on other tokens. The top-10 features in each of the 32 heads sit well above the rest of the pool.

Amplification adds a positive offset to those SAE coefficients during decoding and leaves the residual stream alone. The dose-matched control draws a random feature from the same pool. Newlines per generation is the primary readout; paragraph count and mean word length are surface-quality checks. Doses run $2 \times$, $5 \times$, and $10 \times$ the mean boundary activation, with 400 tokens at temperature 0.7 over 40 prompts.

Results. Amplifying those boundary features reduces line breaks. At the $5 \times$ dose, mean newlines per 400 tokens fall from 16.8 to 11.2. That is a 33% reduction across $n=40$ prompts. Paired t -test $p=0.001$, Cohen’s $d=0.55$ (Fig. 6). The drop is direction-specific.

We selected the $5 \times$ dose post hoc from the full $\{1 \times, 2 \times, 5 \times, 10 \times\}$ sweep, so the effect has to survive multiple-testing correction. Bonferroni across the four doses leaves the $5 \times$ result at $p_{\text{adj}}=0.004$; the $2 \times$ effect ($p_{\text{raw}}=0.015$) does not survive. The dose curve also saturates, so at $10 \times$ the newline count climbs back to 13.4.

Surface metrics move in the predicted direction at smaller amplitude. Paragraph count falls from 7.5 to 6.2. Mean word length shifts from 5.54 to 5.24 characters. The dose-matched random-feature control

Table 4: **Boundary-feature amplification reduces newline rate by 33% on a held-out 4B model.** Generation metrics on Qwen3.5-4B-Base (95% bootstrap CIs, $n=40$ prompts, 400 tokens each). Word length is reported in characters. The primary comparison is $5\times$ amplification vs. baseline.

Condition	Dose	Newlines	Paragraphs	Word length
Baseline	0	16.8 [14.8, 18.9]	7.5 [6.6, 8.5]	5.54
Amplify	$2\times$	12.7 [10.1, 15.5]	6.3 [5.2, 7.4]	5.34
Amplify	$5\times$	11.2 [8.6, 13.9]	6.2 [4.9, 7.4]	5.24
Amplify	$10\times$	13.4 [10.1, 16.8]	7.4 [5.9, 8.9]	5.29
Random	$10\times$	19.0 [17.2, 20.8]	7.8 [7.0, 8.7]	5.50

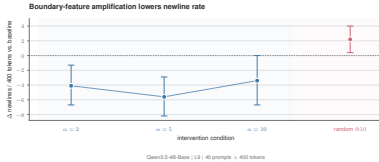


Figure 6: **Boundary-feature amplification changes newline rate in a held-out 4B probe.** Mean newlines per 400 generated tokens on Qwen3.5-4B-Base L9, $n=40$ prompts. Amplifying BilinearSAE features selected by sentence-boundary activation at $5\times$ changes the count from 16.8 to 11.2 (-33% , $p=0.001$); the response saturates and rebounds toward baseline at $10\times$. The dose-matched random-feature control at $10\times$ changes the count in the opposite direction (above baseline). Word-length stays within ± 0.3 characters across conditions (Table 4).

at $10\times$ takes newlines the other way, up to 19.0, above the 16.8 baseline. The boundary-feature direction is selective, not dose-driven.

Controls. In a separate 0.8B experiment, FlatSAE amplification reduces word length (4.86 \rightarrow 3.53) and leaves paragraph count unchanged: the intervention degrades surface quality without shifting document structure. Only BilinearSAE features produced the target newline reduction. FlatSAE and MatrixSAE (a dense-encoder rank-1 SAE on S_t) results come from separate 0.8B pilots with different feature pools and higher dead-feature rates (80% vs. 32%), so they serve as negative controls rather than matched comparisons. The amplification/suppression asymmetry has a structural explanation: TopK activations are nonnegative, so the sparse code has no negative loadings, and suppression can at most clamp a coefficient to zero while amplification can increase it.

A second cell on the same 4B model shows the constraint behind the layer-9 newline result. We repeat the protocol at L12 H8 with a different target behavior: amplifying the top-10 features more active on proper nouns than on other tokens at $5\times$ on 40 prompts of 150 tokens. The capitalized-word rate moves from 0.0862 at baseline to 0.0852, a $\Delta = -0.001$ shift at $d = -0.03$, $p=0.86$ against baseline (reported failure) and $p=0.18$ against a dose-matched random-feature control. The top-10 proper-noun features at L12 H8 have a maximum $|\text{mean_diff}|=0.0047$ between proper-noun and other tokens, an order of magnitude below the layer-9 boundary signal. The L12 H8 dictionary does not contain an atom that separates proper nouns from other tokens, and the signal did not transfer in this cell. Cache generation interventions require an atom whose activation separates the target behavior; this requirement is not automatic across cells.

5 Related Work

Sparse autoencoders, circuits, and causal edits. Transformer SAEs decode the residual stream [Elhage et al., 2022, Bricken et al., 2023, Gao et al., 2025], so their atoms are vectors. The closest non-residual line is transcoders [Dunefsky et al., 2024, Paulo et al., 2025, Marks et al., 2025]: a transcoder substitutes an MLP’s contribution, but that contribution is still a vector. WriteSAE sits at a different intervention site, where the layer writes a matrix; this forces atoms with matching matrix shape. Dictionary learning outside ML has had matrix atoms for decades [Ravishankar et al., 2015, Olshausen and Field, 1996]. A long line of SAE-side variants has changed objectives and decoder families without leaving the residual-stream target [Makhzani and Frey, 2013, Bussmann et al., 2025, Doods and Gauderis, 2025, Koromilas et al., 2026, Engels et al., 2025]. Causal evaluations of these dictionaries [Karvonen et al., 2025, Gurnee et al., 2023, Mueller et al., 2026, Lieberum et al., 2024] and the activation-editing line [Conmy et al., 2023, Geiger et al., 2024, Meng et al., 2023, Wu et al., 2024, 2025, Ameisen et al., 2025, Lindsey et al., 2025] give us our protocol; the difference is that our test perturbs one rank-1 cache write rather than a residual vector. Concurrent rank-sparse attention work [He et al., 2026] asks how rank shapes attention’s own decomposition; for us, rank is set by the host write rule.

Matrix-recurrent states and low-rank structure. Each state-space and hybrid recurrent layer adds something low-rank to its cache every token. Fast-weight programmers [Schmidhuber, 1992, Schlag et al., 2021] introduced the rank-1 outer-product update; linear attention [Katharopoulos et al.,

2020] and test-time-training layers [Sun et al., 2024] reuse the same arithmetic; modern hybrids scale it across RetNet, GLA, Gated DeltaNet, DeltaNet, RWKV-7, Mamba-2, Hedgehog, and mixture-of-memory variants [Sun et al., 2023, Yang et al., 2024a, 2025b, 2024b, Peng et al., 2025, Dao and Gu, 2024, Zhang et al., 2024, Du et al., 2026]. Prior probes of the recurrent state describe its content [Pitorro and Treviso, 2025, Airlangga et al., 2025, Arora et al., 2025, Okpeke and Orvieto, 2025, Sharma et al., 2024] or compress it after the fact [Chang et al., 2025, Nazari and Rusch, 2026]. We target the per-write structure that produced the state instead, by substituting a learned rank-1 atom for the layer’s own write.

The shape of an SAE atom has to match the shape of what the host layer writes. SAE-side and adaptation-side work usually probes residual streams or hidden-state offsets [Paulo et al., 2024, Wang et al., 2025, Hossain et al., 2025, Sunku Mohan et al., 2026, Yap, 2026, Galim et al., 2024], while parameter-side decompositions sparsify weights or Jacobians upstream of the cache [Farnik et al., 2025, Braun et al., 2025, Bushnaq et al., 2025]. We match the atom rank to the host write rule: rank-1 for outer-product writes, diagonal for Mamba-2, and rank-2 for RWKV-7. Mamba-3 [Lahoti et al., 2026] adds new state-input geometries (exponential-trapezoidal, complex, MIMO) that would test the same rule. Our observed $\text{GDN} > \text{RWKV-7} > \text{Mamba-2}$ ordering aligns with the expressivity gap that outer-product corrections open over diagonal-only updates [Siems et al., 2025].

6 Discussion and Conclusion

The main claim is limited but concrete: when the model writes a rank-1 matrix update, a rank-1 SAE atom can often replace that single update. GDN shows the clearest register class and the best fit to the closed-form logit shift ($R^2=0.98$). Mamba-2 and RWKV-7 show weaker alignment, but learned atoms still beat deleting the write at population scale. The replacement test transfers across recurrent families; the GDN gate coefficient does not.

6.1 Limitations and future work

We focus on Qwen3.5-0.8B GDN L9 H4 because its native write is a single rank-1 outer product, the same shape used by WriteSAE atoms. Per-atom identity varies across SAE seeds (less than 1% of atoms match at cosine > 0.9); the register/bundle class is the unit that transfers across seeds. The reported failures below point to a write-aligned loss for 4B, a Mamba-2-specific logit formula, substitutions that handle several active atoms at once, and Mamba-3 atom shapes [Lahoti et al., 2026]. Scaling F412 erasure to multi-feature edits remains open.

6.2 Falsification and observed failures

Four reported failures bound the result: the GDN logit formula does not transfer directly to Mamba-2, the same SAE recipe does not give a 4B firing-level effect, rank-2 atoms give only a small top-1 gain, and the Mamba-2 generation edit fails.

Logit formula outside GDN. The formula $\Delta\ell \approx G \cdot \langle \mathbf{w}_i, \mathbf{q}_t \rangle \cdot \langle \mathbf{v}_i, W_U[\text{tok}] \rangle$ predicts measured effects at $R^2=0.98$ at GDN L9 H4. On Mamba-2 L24 H0 and Qwen3.5-4B L12 H8, the same formula yields negative R^2 (-0.07 and -0.05). Architectures without the same multiplicative gate need their own coefficient form. The partition test and cache replacement transfer across host architectures; the gate coefficient does not.

Larger Qwen model. At Qwen3.5-4B L12 H8 with the same SAE recipe used at 0.8B, atoms beat deleting the write only at chance (48% pooled, $n=600$). The 4B SAE reaches better validation MSE than the 0.8B SAE (5.6×10^{-6} vs 2.2×10^{-5}), so the failure is not under-training. Reconstruction optimizes state recovery; substitution requires write-direction alignment. At scale these objectives decouple, motivating a write-aligned training objective.

Rank-2 top-1 comparison. Independent rank-1 and rank-2 SAEs use different feature-index conventions. A head-to-head test using each SAE’s top-1 atom per firing gives rank-2 a small edge (Cliff’s $\delta = -0.028$, $p < 10^{-71}$, $n=24,600$), with median log-ratio of KL -0.035 . Because GDN writes one rank-1 outer per step, the practical gain is small when replacing one cache write.

Mamba-2 generation edit. Applying the GDN-derived generation edit to Mamba-2 L24 H0 produces no lift in target inclusion across $n=3,600$ trials, with median first-step logp lift ≈ 0 . This failure matches the logit-formula failure outside GDN: the direction is approximate at Mamba-2 and too small to alter greedy generation. Together with the GDN success, it scopes this cache edit to architectures with the same gate and readout structure.

References

- Muhammad Cendekia Airlangga, Hilal AlQuabeh, Munachiso S. Nwadike, and Kentaro Inui. Emergence of primacy and recency effect in Mamba: A mechanistic point of view, 2025. URL <https://arxiv.org/abs/2506.15156>.
- Emmanuel Ameisen, Jack Lindsey, Adam Pearce, Wes Gurnee, Nicholas L. Turner, Brian Chen, Craig Citro, David Abrahams, Shan Carter, Basil Hosmer, Jonathan Marcus, Michael Sklar, Adly Templeton, Trenton Bricken, Callum McDougall, Hoagy Cunningham, Thomas Henighan, Adam Jermyn, Andy Jones, Andrew Persic, Zhenyi Qi, T. Ben Thompson, Sam Zimmerman, Kelley Rivoire, Thomas Conerly, Chris Olah, and Joshua Batson. Circuit tracing: Revealing computational graphs in language models. Transformer Circuits Thread, mar 2025. URL <https://transformer-circuits.pub/2025/attribution-graphs/methods.html>.
- Aryaman Arora, Neil Rathi, Nikil Roashan Selvam, Róbert Csordás, Dan Jurafsky, and Christopher Potts. Mechanistic evaluation of transformers and state space models, 2025. URL <https://arxiv.org/abs/2505.15105>.
- Jimmy Ba, Geoffrey Hinton, Volodymyr Mnih, Joel Z. Leibo, and Catalin Ionescu. Using fast weights to attend to the recent past. In *Advances in Neural Information Processing Systems (NeurIPS)*, 2016.
- Dan Braun, Lucius Bushnaq, Stefan Heimersheim, Jake Mendel, and Lee Sharkey. Interpretability in parameter space: Minimizing mechanistic description length with attribution-based parameter decomposition, 2025. URL <https://arxiv.org/abs/2501.14926>.
- Trenton Bricken, Adly Templeton, Joshua Batson, Brian Chen, Adam Jermyn, Tom Conerly, Nick Turner, Cem Anil, Carson Denison, Amanda Askell, Robert Lasenby, Yifan Wu, Shauna Kravec, Nicholas Schiefer, Tim Maxwell, Nicholas Joseph, Zac Hatfield-Dodds, Alex Tamkin, Karina Nguyen, Brayden McLean, Josiah E. Burke, Tristan Hume, Shan Carter, Tom Henighan, and Christopher Olah. Towards monosemanticity: Decomposing language models with dictionary learning. *Transformer Circuits Thread*, 2023. URL <https://transformer-circuits.pub/2023/monosemantic-features>.
- Lucius Bushnaq, Dan Braun, and Lee Sharkey. Stochastic parameter decomposition, 2025. URL <https://arxiv.org/abs/2506.20790>.
- Bart Bussmann, Patrick Leask, and Neel Nanda. BatchTopK sparse autoencoders, 2024. URL <https://arxiv.org/abs/2412.06410>.
- Bart Bussmann, Noa Nabeshima, Adam Karvonen, and Neel Nanda. Learning multi-level features with matryoshka sparse autoencoders, 2025. URL <https://arxiv.org/abs/2503.17547>.
- Chi-Chih Chang, Chien-Yu Lin, Yash Akhauri, Wei-Cheng Lin, Kai-Chiang Wu, Luis Ceze, and Mohamed S. Abdelfattah. xKV: Cross-layer SVD for KV-cache compression, 2025. URL <https://arxiv.org/abs/2503.18893>.
- Arthur Conmy, Augustine Mavor-Parker, Aengus Lynch, Stefan Heimersheim, and Adrià Garriga-Alonso. Towards automated circuit discovery for mechanistic interpretability. In *Advances in Neural Information Processing Systems (NeurIPS)*, 2023.
- Valérie Costa, Thomas Fel, Ekdeep Singh Lubana, Bahareh Tolooshams, and Demba Ba. Evaluating sparse autoencoders: From shallow design to matching pursuit, 2025. URL <https://arxiv.org/abs/2506.05239>.
- Hoagy Cunningham, Aidan Ewart, Logan Riggs, Robert Huben, and Lee Sharkey. Sparse autoencoders find highly interpretable features in language models. In *International Conference on Learning Representations*, 2024.
- Tri Dao and Albert Gu. Transformers are SSMS: Generalized models and efficient algorithms through structured state space duality. *arXiv preprint arXiv:2405.21060*, 2024. URL <https://arxiv.org/abs/2405.21060>.
- Thomas Dooms and Ward Gauderis. Finding manifolds with bilinear autoencoders. *arXiv preprint arXiv:2510.16820*, 2025. URL <https://arxiv.org/abs/2510.16820>.

- Jusen Du, Weigao Sun, Disen Lan, Jiayi Hu, and Yu Cheng. MoM: Linear sequence modeling with mixture-of-memories, 2026. URL <https://arxiv.org/abs/2502.13685>.
- Jacob Dunefsky, Philippe Chlenski, and Neel Nanda. Transcoders find interpretable LLM feature circuits. *arXiv preprint arXiv:2406.11944*, 2024. URL <https://arxiv.org/abs/2406.11944>.
- Nelson Elhage, Tristan Hume, Catherine Olsson, Nicholas Schiefer, Tom Henighan, Shauna Kravec, Zac Hatfield-Dodds, Robert Lasenby, Dawn Drain, Carol Chen, Roger Grosse, Sam McCandlish, Jared Kaplan, Dario Amodei, Martin Wattenberg, and Christopher Olah. Toy models of superposition, 2022. URL <https://arxiv.org/abs/2209.10652>.
- Joshua Engels, Eric J. Michaud, Isaac Liao, Wes Gurnee, and Max Tegmark. Not all language model features are one-dimensionally linear. *arXiv preprint arXiv:2405.14860*, 2025. URL <https://arxiv.org/abs/2405.14860>.
- Lucy Farnik, Tim Lawson, Conor Houghton, and Laurence Aitchison. Jacobian sparse autoencoders: Sparsify computations, not just activations, 2025. URL <https://arxiv.org/abs/2502.18147>.
- Kevin Galim, Wonjun Kang, Yuchen Zeng, Hyung Il Koo, and Kangwook Lee. Parameter-efficient fine-tuning of state space models, 2024. URL <https://arxiv.org/abs/2410.09016>.
- Leo Gao, Tom Dupré la Tour, Henk Tillman, Gabriel Goh, Rajan Troll, Alec Radford, Ilya Sutskever, Jan Leike, and Jeffrey Wu. Scaling and evaluating sparse autoencoders. *arXiv preprint arXiv:2406.04093*, 2025. URL <https://arxiv.org/abs/2406.04093>.
- Atticus Geiger, Zhengxuan Wu, Christopher Potts, Thomas Icard, and Noah D. Goodman. Finding alignments between interpretable causal variables and distributed neural representations. In *Conference on Causal Learning and Reasoning (CLear)*, 2024.
- Aaron Gokaslan and Vanya Cohen. Openwebtext corpus. <https://skylion007.github.io/OpenWebTextCorpus>, 2019. URL <https://skylion007.github.io/OpenWebTextCorpus>.
- Wes Gurnee, Neel Nanda, Matthew Pauly, Katherine Harvey, Dmitrii Troitskii, and Dimitris Bertsimas. Finding neurons in a haystack: Case studies with sparse probing, 2023. URL <https://arxiv.org/abs/2305.01610>.
- Zhengfu He, Junxuan Wang, Rui Lin, Xuyang Ge, Wentao Shu, Qiong Tang, Junping Zhang, and Xipeng Qiu. Towards understanding the nature of attention with low-rank sparse decomposition. In *International Conference on Learning Representations (ICLR)*, 2026.
- Tamanna Hossain, Robert L. Logan IV, Ganesh Jagadeesan, Sameer Singh, Joel Tetreault, and Alejandro Jaimes. Characterizing Mamba’s selective memory using auto-encoders. In *Findings of IJCNLP-AACL*, 2025.
- Jiayi Hu, Yongqi Pan, Jusen Du, Disen Lan, Xiaqiang Tang, Qingsong Wen, Yuxuan Liang, and Weigao Sun. Comba: Improving bilinear RNNs with closed-loop control, 2025. URL <https://arxiv.org/abs/2506.02475>.
- Thomas Jiralerspong and Trenton Bricken. Cross-architecture model diffing with crosscoders: Unsupervised discovery of differences between LLMs, 2026. URL <https://arxiv.org/abs/2602.11729>.
- Adam Karvonen, Can Rager, Johnny Lin, Curt Tigges, Joseph Bloom, David Chanin, Yeu-Tong Lau, Eoin Farrell, Callum McDougall, Kola Ayonrinde, Demian Till, Matthew Wearden, Arthur Conmy, Samuel Marks, and Neel Nanda. SAEBench: A comprehensive benchmark for sparse autoencoders in language model interpretability. In *Proceedings of the 42nd International Conference on Machine Learning (ICML)*, volume 267 of *PMLR*, pages 29223–29264, 2025.
- Angelos Katharopoulos, Apoorv Vyas, Nikolaos Pappas, and François Fleuret. Transformers are RNNs: Fast autoregressive transformers with linear attention. In *International Conference on Machine Learning (ICML)*, pages 5156–5165, 2020.
- Panagiotis Koromilas, Andreas D. Demou, James Oldfield, Yannis Panagakis, and Mihalis A. Nicolaou. PolySAE: Modeling feature interactions in sparse autoencoders via polynomial decoding. *arXiv preprint arXiv:2602.01322*, 2026. URL <https://arxiv.org/abs/2602.01322>.

- Aakash Lahoti, Kevin Y. Li, Berlin Chen, Caitlin Wang, Aviv Bick, J. Zico Kolter, Tri Dao, and Albert Gu. Mamba-3: Improved sequence modeling using state space principles. In *International Conference on Learning Representations (ICLR)*, 2026.
- Michael Lan, Philip Torr, Austin Meek, Ashkan Khakzar, David Krueger, and Fazl Barez. Quantifying feature space universality across large language models via sparse autoencoders, 2024. URL <https://arxiv.org/abs/2410.06981>.
- Tom Lieberum, Senthooan Rajamanoharan, Arthur Conmy, Lewis Smith, Nicolas Sonnerat, Vikrant Varma, János Kramár, Anca Dragan, Rohin Shah, and Neel Nanda. Gemma scope: Open sparse autoencoders everywhere all at once on Gemma 2. *arXiv preprint arXiv:2408.05147*, 2024. URL <https://arxiv.org/abs/2408.05147>.
- Jack Lindsey, Wes Gurnee, Emmanuel Ameisen, Brian Chen, Adam Pearce, Nicholas L. Turner, Chris Olah, and Joshua Batson. On the biology of a large language model. Transformer Circuits Thread, mar 2025. URL <https://transformer-circuits.pub/2025/attribution-graphs/biology.html>.
- Alireza Makhzani and Brendan Frey. k-sparse autoencoders, 2013. URL <https://arxiv.org/abs/1312.5663>.
- Samuel Marks, Can Rager, Eric J. Michaud, Yonatan Belinkov, David Bau, and Aaron Mueller. Sparse feature circuits: Discovering and editing interpretable causal graphs in language models. In *International Conference on Learning Representations*, 2025.
- Kevin Meng, Arnab Sen Sharma, Alex Andonian, Yonatan Belinkov, and David Bau. Mass-editing memory in a transformer. In *International Conference on Learning Representations (ICLR)*, 2023.
- Aaron Mueller, Atticus Geiger, Sarah Wiegrefe, Dana Arad, Iván Arcuschin, Adam Belfki, Yik Siu Chan, Jaden Fiotto-Kaufman, Tal Haklay, Michael Hanna, Jing Huang, Rohan Gupta, Yaniv Nikankin, Hadas Orgad, Nikhil Prakash, Anja Reusch, Aruna Sankaranarayanan, Shun Shao, Alessandro Stolfo, Martin Tutek, Amir Zur, David Bau, and Yonatan Belinkov. MIB: A mechanistic interpretability benchmark, 2026. URL <https://arxiv.org/abs/2504.13151>.
- Philipp Nazari and T. Konstantin Rusch. The key to state reduction in linear attention: A rank-based perspective, 2026. URL <https://arxiv.org/abs/2602.04852>.
- Destiny Okpeke and Antonio Orvieto. Revisiting associative recall in modern recurrent models, 2025. URL <https://arxiv.org/abs/2508.19029>.
- Bruno A. Olshausen and David J. Field. Emergence of simple-cell receptive field properties by learning a sparse code for natural images. *Nature*, 381(6583):607–609, 1996. doi: 10.1038/381607a0.
- Gonçalo Paulo and Nora Belrose. Sparse autoencoders trained on the same data learn different features, 2026. URL <https://arxiv.org/abs/2501.16615>.
- Gonçalo Paulo, Thomas Marshall, and Nora Belrose. Does transformer interpretability transfer to rnns? *arXiv preprint arXiv:2404.05971*, 2024. URL <https://arxiv.org/abs/2404.05971>.
- Gonçalo Paulo, Stepan Shabalín, and Nora Belrose. Transcoders beat sparse autoencoders for interpretability, 2025. URL <https://arxiv.org/abs/2501.18823>.
- Bo Peng, Ruichong Zhang, Daniel Goldstein, Eric Alcaide, Xingjian Du, Haowen Hou, Jiaju Lin, Jiaying Liu, Janna Lu, William Merrill, Guangyu Song, Kaifeng Tan, Saiteja Utpala, Nathan Wilce, Johan S. Wind, Tianyi Wu, Daniel Wuttke, and Christian Zhou-Zheng. RWKV-7 “Goose” with expressive dynamic state evolution. In *Conference on Language Modeling (COLM)*, 2025.
- Hugo Pitorro and Marcos Treviso. LaTIM: Measuring latent token-to-token interactions in Mamba models, 2025. URL <https://arxiv.org/abs/2502.15612>.
- Senthooan Rajamanoharan, Arthur Conmy, Lewis Smith, Tom Lieberum, Vikrant Varma, János Kramár, Rohin Shah, and Neel Nanda. Improving dictionary learning with gated sparse autoencoders. *arXiv preprint arXiv:2404.16014*, 2024a. URL <https://arxiv.org/abs/2404.16014>.

- Senthooran Rajamanoharan, Tom Lieberum, Nicolas Sonnerat, Arthur Conmy, Vikrant Varma, János Kramár, and Neel Nanda. Jumping ahead: Improving reconstruction fidelity with JumpReLU sparse autoencoders. *arXiv preprint arXiv:2407.14435*, 2024b. URL <https://arxiv.org/abs/2407.14435>.
- Saiprasad Ravishankar, Raj Rao Nadakuditi, and Jeffrey A. Fessler. Efficient sum of outer products dictionary learning (SOUP-DIL) - the ℓ_0 method, 2015. URL <https://arxiv.org/abs/1511.08842>.
- Adam Scherlis, Kshitij Sachan, Adam S. Jermyn, Joe Benton, and Buck Shlegeris. Polysemanticity and capacity in neural networks, 2022. URL <https://arxiv.org/abs/2210.01892>.
- Imanol Schlag, Kazuki Irie, and Jürgen Schmidhuber. Linear transformers are secretly fast weight programmers. In *International Conference on Machine Learning (ICML)*, 2021.
- Jürgen Schmidhuber. Learning to control fast-weight memories: An alternative to dynamic recurrent networks. *Neural Computation*, 4(1):131–139, 1992. doi: 10.1162/neco.1992.4.1.131.
- Arnab Sen Sharma, David Atkinson, and David Bau. Locating and editing factual associations in Mamba. In *Conference on Language Modeling (COLM)*, 2024.
- Julien Siems, Timur Carstensen, Arber Zela, Frank Hutter, Massimiliano Pontil, and Riccardo Grazi. Deltaproduct: Improving state-tracking in linear rnns via householder products, 2025. URL <https://arxiv.org/abs/2502.10297>.
- Xiaoqing Sun, Alessandro Stolfo, Joshua Engels, Ben Wu, Senthooran Rajamanoharan, Mrinmaya Sachan, and Max Tegmark. Dense SAE latents are features, not bugs, 2025. URL <https://arxiv.org/abs/2506.15679>.
- Yu Sun, Xinhao Li, Karan Dalal, Jiarui Xu, Arjun Vikram, Genghan Zhang, Yann Dubois, Xinlei Chen, Xiaolong Wang, Sanmi Koyejo, Tatsunori Hashimoto, and Carlos Guestrin. Learning to (learn at test time): RNNs with expressive hidden states. *arXiv preprint arXiv:2407.04620*, 2024. URL <https://arxiv.org/abs/2407.04620>.
- Yutao Sun, Li Dong, Shaohan Huang, Shuming Ma, Yuqing Xia, Jilong Xue, Jianyong Wang, and Furu Wei. Retentive network: A successor to transformer for large language models, 2023. URL <https://arxiv.org/abs/2307.08621>.
- Vamshi Sunku Mohan, Kaustubh Gupta, Aneesha Das, and Chandan Singh. Interpreting and steering state-space models via activation subspace bottlenecks. *arXiv preprint arXiv:2602.22719*, 2026. URL <https://arxiv.org/abs/2602.22719>.
- Adly Templeton, Tom Conerly, Jonathan Marcus, Jack Lindsey, Trenton Bricken, Brian Chen, Adam Pearce, Craig Citro, Emmanuel Ameisen, Andy Jones, Hoagy Cunningham, Nicholas L. Turner, Callum McDougall, Monte MacDiarmid, C. Daniel Freeman, Theodore R. Sumers, Edward Rees, Joshua Batson, Adam Jermyn, Shan Carter, Chris Olah, and Tom Henighan. Scaling monosemanticity: Extracting interpretable features from Claude 3 Sonnet. *Transformer Circuits Thread*, 2024. URL <https://transformer-circuits.pub/2024/scaling-monosemanticity>.
- Junxuan Wang, Xuyang Ge, Wentao Shu, Qiong Tang, Yunhua Zhou, Zhengfu He, and Xipeng Qiu. Towards universality: Studying mechanistic similarity across language model architectures. *arXiv preprint arXiv:2410.06672*, 2025. URL <https://arxiv.org/abs/2410.06672>.
- Zhengxuan Wu, Aryaman Arora, Zheng Wang, Atticus Geiger, Dan Jurafsky, Christopher D. Manning, and Christopher Potts. ReFT: Representation finetuning for language models. In *Advances in Neural Information Processing Systems (NeurIPS)*, 2024.
- Zhengxuan Wu, Aryaman Arora, Atticus Geiger, Zheng Wang, Jing Huang, Dan Jurafsky, Christopher D. Manning, and Christopher Potts. AxBench: Steering LLMs? Even simple baselines outperform sparse autoencoders, 2025. URL <https://arxiv.org/abs/2501.17148>.
- An Yang, Anfeng Li, Baosong Yang, Beichen Zhang, Binyuan Hui, Bo Zheng, Bowen Yu, Chang Gao, Chengen Huang, Chenxu Lv, Chujie Zheng, Dayiheng Liu, Fan Zhou, Fei Huang, Feng Hu, Hao Ge, Haoran Wei, Huan Lin, Jialong Tang, Jian Yang, Jianhong Tu, Jianwei Zhang, Jianxin Yang, Jiayi Yang, Jing Zhou, Jingren Zhou, Junyang Lin, Kai Dang, Keqin Bao, Kexin Yang,

- Le Yu, Lianghao Deng, Mei Li, Mingfeng Xue, Mingze Li, Pei Zhang, Peng Wang, Qin Zhu, Rui Men, Ruize Gao, Shixuan Liu, Shuang Luo, Tianhao Li, Tianyi Tang, Wenbiao Yin, Xingzhang Ren, Xinyu Wang, Xinyu Zhang, Xuancheng Ren, Yang Fan, Yang Su, Yichang Zhang, Yinger Zhang, Yu Wan, Yuqiong Liu, Zekun Wang, Zeyu Cui, Zhenru Zhang, Zhipeng Zhou, and Zihan Qiu. Qwen3 technical report, 2025a. URL <https://arxiv.org/abs/2505.09388>.
- Songlin Yang and Yu Zhang. Flash linear attention. <https://github.com/sustcsonglin/flash-linear-attention>, 2024. URL <https://github.com/sustcsonglin/flash-linear-attention>.
- Songlin Yang, Bailin Wang, Yikang Shen, Rameswar Panda, and Yoon Kim. Gated linear attention transformers with hardware-efficient training. *arXiv preprint arXiv:2312.06635*, 2024a. URL <https://arxiv.org/abs/2312.06635>.
- Songlin Yang, Bailin Wang, Yu Zhang, Yikang Shen, and Yoon Kim. Parallelizing linear transformers with the delta rule over sequence length. In *Advances in Neural Information Processing Systems*, pages 115491–115522, 2024b. doi: 10.52220/079017-3668.
- Songlin Yang, Jan Kautz, and Ali Hatamizadeh. Gated delta networks: Improving Mamba2 with delta rule. In *International Conference on Learning Representations (ICLR)*, 2025b.
- Jia Qing Yap. Behavioral steering in a 35B MoE language model via SAE-decoded probe vectors: One agency axis, not five traits. *arXiv preprint arXiv:2603.16335*, 2026. URL <https://arxiv.org/abs/2603.16335>.
- Fred Zhang and Neel Nanda. Towards best practices of activation patching in language models: Metrics and methods, 2024. URL <https://arxiv.org/abs/2309.16042>.
- Michael Zhang, Kush Bhatia, Hermann Kumbong, and Christopher Ré. The hedgehog & the porcupine: Expressive linear attentions with softmax mimicry. In *International Conference on Learning Representations (ICLR)*, 2024.

A Derivation of the Three-Factor Logit Factorization

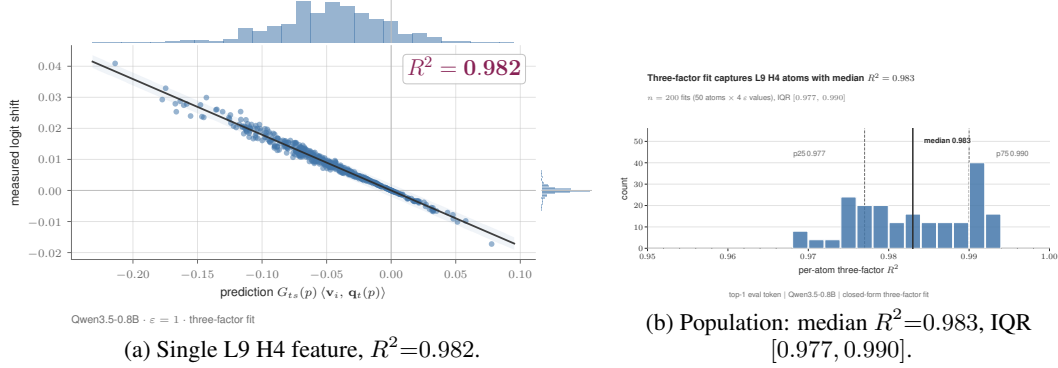


Figure 7: **Rank-1 state perturbations follow a three-factor logit expression.** (a) Measured logit shift vs. predicted $G_{t_0 \rightarrow t}(c) \cdot \langle \mathbf{w}_i, \mathbf{q}_t(c) \rangle \cdot \langle \mathbf{v}_i, W_U[\text{tok}] \rangle$ for one L9 H4 feature. (b) Per-atom three-factor R^2 across $n=200$ fits (50 atoms $\times 4 \epsilon$).

Under a rank-1 perturbation of the cached Gated DeltaNet state at reference position $t_0 < t$ along feature i with decoder pair $(\mathbf{v}_i, \mathbf{w}_i)$,

$$\Delta \ell_{\text{tok}}(c, i, t) \approx G_{t_0 \rightarrow t}(c) \cdot \langle \mathbf{w}_i, \mathbf{q}_t(c) \rangle \cdot \langle \mathbf{v}_i, W_U[\text{tok}] \rangle, \quad (4)$$

where \mathbf{q}_t is the query at t , $W_U[\text{tok}]$ the output-embedding row, and $G_{t_0 \rightarrow t}$ a prompt-/position-specific gate product.

Setup. Let S_{t_0} be the cached Gated DeltaNet state at reference position t_0 for one head at one layer. A rank-1 perturbation along feature i 's decoder writes $S_{t_0} \mapsto S_{t_0} + \epsilon \mathbf{v}_i \mathbf{w}_i^\top$. We propagate through the remaining Gated DeltaNet recurrence to t , read against \mathbf{q}_t , pass through residual, attention, and MLP layers, and project to logits via W_U .

State propagation. The native gated delta rule [Yang et al., 2025b] is

$$S_{s+1} = \alpha_{s+1}(c)(I - \beta_{s+1}(c) \mathbf{k}_{s+1}(c) \mathbf{k}_{s+1}(c)^\top) S_s + \beta_{s+1}(c) \mathbf{k}_{s+1}(c) \mathbf{v}_{s+1}(c)^\top.$$

Differencing perturbed and native trajectories cancels the additive write and leaves

$$\delta S_{s+1} = \alpha_{s+1}(c)(I - \beta_{s+1}(c) \mathbf{k}_{s+1}(c) \mathbf{k}_{s+1}(c)^\top) \delta S_s, \quad \delta S_{t_0} = \epsilon \mathbf{v}_i \mathbf{w}_i^\top.$$

Multiplying by the rank-one correction gives a cross term of magnitude $\beta_{s+1} \langle \mathbf{w}_i, \mathbf{k}_{s+1} \rangle$. For a register atom, \mathbf{w}_i aligns with one prompt-restricted subset of keys; on every other step the cross term is small, so the correction acts like the identity on δS_s and leaves the scalar gate $\alpha_{s+1}(c)$. Iterating,

$$\delta S_t \approx \epsilon \left[\prod_{s=t_0+1}^t \alpha_s(c) \right] \mathbf{v}_i \mathbf{w}_i^\top \equiv \epsilon G_{t_0 \rightarrow t}^\alpha(c) \mathbf{v}_i \mathbf{w}_i^\top.$$

The reduction is empirical: residual cross-term mass is accounted for by the same prompt-dependent prefactor we absorb into $G_{t_0 \rightarrow t}(c)$. A scalar gate cannot mix the rank-1 outer with anything else, so the perturbation stays rank-1; only its norm decays.

Read through the head. At position t the head reads $\mathbf{o}_t = S_t \mathbf{q}_t$. Hitting that read with δS_t :

$$\delta \mathbf{o}_t = \epsilon G_{t_0 \rightarrow t}^\alpha(c) \cdot \langle \mathbf{w}_i, \mathbf{q}_t(c) \rangle \cdot \mathbf{v}_i.$$

The output-space perturbation is pinned in direction to \mathbf{v}_i regardless of prompt; the prompt only sets magnitude.

Downstream path to logits. Write $J(c, t)$ for the Jacobian from head output (L, t) to the final residual stream at t . To first order in ϵ ,

$$\Delta \ell_{\text{tok}}(c, i, t) = \epsilon G_{t_0 \rightarrow t}^\alpha(c) \cdot \langle \mathbf{w}_i, \mathbf{q}_t(c) \rangle \cdot \langle J(c, t) \mathbf{v}_i, W_U[\text{tok}] \rangle.$$

Eq. 4 substitutes \mathbf{v}_i for $J(c, t) \mathbf{v}_i$, absorbing the rotation-and-rescaling into G . Two empirical observations support the substitution: encoder/decoder cosine for register atoms is 0.94 ± 0.02 on the DeltaNet probe (0.65 ± 0.10 at Qwen L9 H4), and we observe 0 sign flips of $\Delta \ell$ relative to $\text{sign} \langle \mathbf{w}_i, \mathbf{q}_t \rangle$ across 10,000 trials (Wilson upper bound 0.04%). A prompt-dependent rotation off the unembed direction would flip signs.

Empirical G . G depends on activation statistics through $J(c, t)$, fit numerically: one scalar per (prompt, feature, eval-token) triple, recovered by least squares. The fitted G tracks $\prod \alpha_s$ to first order with a small prompt-level residual. Median per-feature $R^2=0.98$ at L9 H4 (Figure 7).

Gate factor in Qwen3.5 Gated DeltaNet. The Qwen3.5 Gated DeltaNet block computes $g_s = -\exp(A_h^{\log}) \cdot \text{softplus}(a_s(c) + b_h^{\text{dt}})$; forget gate $\alpha_s = \exp(g_s)$, write gate $\beta_s = \sigma(b_s)$, both scalar per head. For horizon h , $G_{t_0 \rightarrow t_0+h}^\alpha(c) = \prod_{s=t_0+1}^{t_0+h} \exp(g_s(c))$. The full G multiplies this by $\|J(c, t)\mathbf{v}_i\|/\|\mathbf{v}_i\|$ and the cosine between \mathbf{u}_i and \mathbf{v}_i ; none depends on the eval token, so G enters as a single scalar.

Population audit. Over 50×4 (atom, ε) cells with $\varepsilon \in \{0.1, 0.3, 1.0, 3.0\}$, 500 prompts each: median $R^2=0.983$, IQR $[0.977, 0.990]$, 10th percentile 0.974; all 200 cells exceed $R^2=0.95$. Top-2-top-5 eval-token ranks hold $R^2 \in [0.983, 0.984]$; tail logits degrade to $R^2 \approx 0.05$ at rank 50. The expression fits dominant logit shifts; tail contributions are higher-order Taylor terms.

Scope. The approximation is a first-order Taylor expansion around $\varepsilon = 0$, supported by selectivity being ε -invariant to four decimals across $\varepsilon \in [0.1, 3]$ (Section 3.2). Host-architecture analogs at Mamba-2 L24 H0 and Qwen3.5-4B L12 H8 yield negative R^2 , identifying G as the architecture-specific component (Section 6.2).

B SAE-Family Invariance of the Partition

The partition in Section 3.2 uses BatchTopK [Bussmann et al., 2024]. A JumpReLU bilinear SAE [Rajamanoharan et al., 2024b] retrained on the same Qwen3.5-0.8B L9 H4 GDN state (matched optimizer/LR/20-epoch budget; $\lambda_{\text{sparsity}}=10^{-5}$, $\theta_0=10^{-4}$, bandwidth $10^{-3} \rightarrow 10^{-5}$ cosine; converges to Val MSE 5.71×10^{-6} , $L_0=1,142$, zero dead) reproduces the partition.

Table 5: **Partition is stable under a JumpReLU sparsity swap and reaches $105\times$ within-SAE separation against BatchTopK’s $29\times$.** Both objectives recover the same register class on the same GDN state; JumpReLU’s adaptive threshold uses every feature. Qwen3.5-0.8B L9 H4; $n_f=2048$; 20 epochs.

SAE objective	$n_{\text{reg}} / n_{\text{bun}}$	dead	register cos	bundle cos	reg/bun
BatchTopK ($k=32, L_0=32$)	222/94	1,732	0.262	0.009	$29\times$
JumpReLU ($L_0 \approx 1,142$)	1,259/773	16	0.189	0.0018	$105\times$

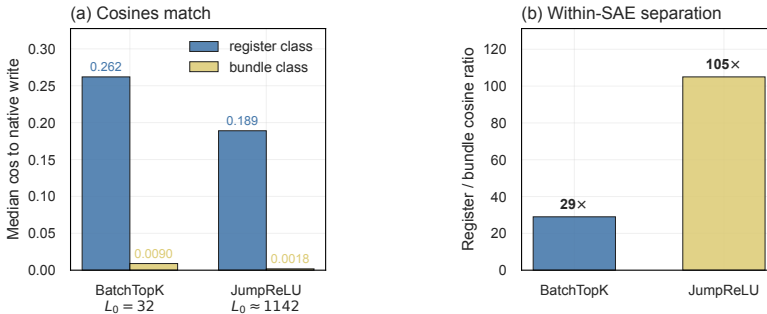


Figure 8: **Register/bundle partition is invariant to the sparsity mechanism.** (a) Median cosine to the native write under BatchTopK ($L_0=32$) and JumpReLU ($L_0 \approx 1,142$). Register cosines stay within 28%; bundle cosines are near zero in both. (b) Within-SAE register/bundle cosine ratio: JumpReLU $105\times$ vs BatchTopK $29\times$.

Gated SAE (negative). Gated [Rajamanoharan et al., 2024a] under hard, hard+STE, and soft-sigmoid ($\tau=0.1$) gate indicators all failed: hard converged to $L_0 \rightarrow 0$ in epoch 1, STE stalled at $L_0 \approx 0.5$, and soft-sigmoid gave $7\times$ worse MSE at matched L_0 . BatchTopK and JumpReLU are the two stable objectives.

Mamba-2 random rank-1 baseline. For Mamba-2’s diagonal-SSM substitution, the matched random rank-1 control samples ($w_{\text{head}}, w_{\text{state}}$) independently from the empirical per-coordinate distribution of native updates at the firing position, then renormalizes the resulting outer product to match the Frobenius norm of the native diagonal write. The single-cell number (82.85%, $n=2,367$) is superseded by the 100-atom population sweep at 88.08% in Section 3.3.

C Full Encoder-Swap MSE Comparison

Rank-1 as architectural match. A Gated DeltaNet write adds exactly one rank-1 outer $\mathbf{k}_t \mathbf{v}_t^\top$ per token; a rank-1 dictionary atom $\mathbf{v}_i \mathbf{w}_i^\top$ corresponds one-to-one with one cache event, and the

Table 6: **The architecture-matched decoder gives the largest measured substitution-success gain where the native write is least rank-1.** WriteSAE register cosine measures the trained-dictionary side of the rank gradient (Section 3.3). Substitution-success gap is the percent of firings where the WriteSAE atom beats deleting the write minus the corresponding FlatSAE+top- K -SVD rate on the same firing set. $n_f=2,048$, $k=32$, seed 42, 20 epochs; matched-Frobenius substitution; protocol in App. F.4.

Substrate (write rule)	WriteSAE reg. cos	WriteSAE vs FlatSAE+SVD Δ	n_{records}
Gated DeltaNet (rank-1 outer)	0.262	-0.11pp (91.25% vs 91.36%) [†]	1,851
RWKV-7 (rank-2 outer + erase)	0.180	-2.52pp (45.3% vs 47.8%)*	6,591
Mamba-2 (diagonal SSM)	0.0575	+6.55pp (82.85% vs 76.30%)	2,367

[†]Gated DeltaNet gate decay already rank-1 dominates the state, so SVD top-1 of a flat-SAE atom recovers the same direction the trained dictionary picks; the two methods tie. *Both RWKV-7 substitutions are at the deletion floor on this cell (45.3% and 47.8% against a 50% coin-flip baseline).

Table 7: **Rank-1 reconstruction is within 8% of the unconstrained flat upper bound at L1/L9 and 1.75 \times worse at the diffuse L17.** Layer-averaged validation MSE ($\times 10^{-5}$, 16 heads, 3 seeds) across spectra spanning $\sigma_1/\sigma_2 \approx 12$ to 3.0. Bold: lowest per layer. Flat-dense atoms in $\mathbb{R}^{128 \times 128}$ span the full state and mix many native writes per feature. Qwen3.5-0.8B; $n_f=2048$; $k=32$; 20 epochs.

	Layer 1 ($\sigma_1/\sigma_2 \approx 12$)	Layer 9 (6.8)	Layer 17 (3.0)
Flat (dense enc., dense dec.)	2.61	2.58	30.1
Rank-1 (dense enc., rank-1 dec.)	2.83	2.69	52.8
Bilinear (bilinear enc., rank-1 dec.)	4.07	3.09	54.0
Bilinear-flat (bilinear enc., dense dec.)	3.93	3.35	39.0
Tied bilinear (bilinear enc., tied rank-1)	7.63	5.98	80.5

substitution test of Section 3.2 patches exactly that event. A rank- r atom patches r writes per firing; a flat dense atom mixes up to 128 writes per feature. The flat upper bound beats rank-1 by only 8% at L1/L9 despite using $60\times$ more decoder parameters per atom, and by $1.75\times$ at the diffuse L17. The rank-1 prior trades reconstruction MSE for resolution of the write primitive.

Parameter formulas ($d_k=d_v=128$, $d_{\text{in}}=d_k d_v=16,384$): **FlatSAE** = $2n_f d_{\text{in}} + n_f + d_{\text{in}}$; **WriteSAE** = $n_f d_{\text{in}} + n_f(d_k + d_v) + n_f + d_k d_v$; **BilinearSAE** = $4n_f d_k + n_f + d_k d_v$.

D Hyperparameters

Defaults at `core/train.py`; per-experiment scripts override only the deviations. All runs: Adam; MSE reconstruction with optional auxiliary dead-feature term ($\lambda_{\text{aux}}=10^{-2}$, $k_{\text{aux}}=256$); decoder column re-norm every 100 steps; resampling every 250 steps for atoms inactive ≥ 100 steps; 80/20 split with split seed = weight-init seed; FP32 SAE params on BF16-cast activations.

Table 8: **Per-architecture training configuration.** Shared defaults (Adam, 80/20 split, decoder re-norm every 100 steps, resample every 250 steps after 100-step inactivity) apply throughout.

	GDN (Qwen3.5-0.8B)	GDN (Qwen3.5-4B)	DeltaNet-1.3B	Mamba-2-370M	GLA-1.3B
Source script	sweeps/	run_9pager_overnight	run_deltanet_validation	mamba2/mamba2_sae_experiment	run_gla_validation
Layers extracted	0.2,5,9,13,17,21	matched (L12)	1,12,22	0.6,14,31,46,47	1,12,22
Heads per layer	all (16)	all	head 0	multi-head sweep	head 0
Peak / Min LR	$3 \times 10^{-4} / 3 \times 10^{-5}$	same	same	same	same
Schedule	cosine + warmup	cosine + warmup	cosine + warmup	cosine + warmup	cosine + warmup
Warmup steps	50	50	50	100	50
Batch / Epochs	256 / 20	256 / 20	256 / 20	128 / 50	256 / 20
Sparsity / k	TopK or BatchTopK / 32	TopK / 32	TopK / 32	TopK / 32	TopK / 32
n_{features} / Decoder rank	2048 / 1	2048 / 1	2048 / 1	2048 / 1	2048 / 1
Seeds	{0, 1, 42}	{0, 1, 42}	{0, 1, 2}	{0, 1, 42}	{0, 1, 2}
Extraction (seq. len / #)	1024 / up to 5,000	1024 / matched	1024 / 5,000	1024 / 5,000	1024 / 5,000

Mamba-2 deviation. Per-head $d_{\text{state}}=128$ produces a larger flat input than GDN; pilots had not converged at 20 epochs, so we extend to 50 epochs at batch 128, 100 warmup. Every other arch uses the GDN default block. All training scripts log the git HEAD SHA into `config.json`.

Training-budget control. At 5×10^5 states/head (5K corpus, 20 epochs) the dead-feature ordering reverses to MatrixSAE 83.6% < FlatSAE 86.6% < BilinearSAE 93.3%; at 5×10^6 states/head with 200 epochs the matched-cohort ordering returns (BilinearSAE 85.8% < FlatSAE 93.4% < MatrixSAE 94.0%). The 5K corpus has covariance effective rank 70.2 vs 74.7 at 50K and the same $\sigma_1/\sigma_2=5.998$, so the crossover is a training-dynamics effect, not a coverage gap. BilinearSAE’s parameter-matched control in Section 3.2 ($5.5\times$ worse downstream PPL at the same 8.4M budget) holds across schedules.

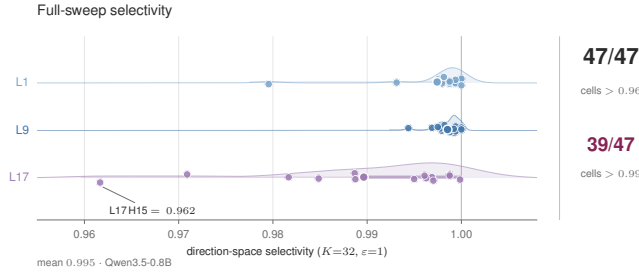


Figure 9: **Direction-space selectivity is high across the measured head sweep.** Each dot is one (L, H) cell; horizontal position is per-cell mean selectivity, filled dot per-layer mean. Sweep $L \in \{1, 9, 17\} \times H \in \{0..15\}$ against matched-norm random rank-1 directions; L17 H14 excluded for upstream-cache corruption (47/48). Mean 0.9953, 39/47 cells exceed 0.99. Qwen3.5-0.8B; $K=32$; $\epsilon=1$.

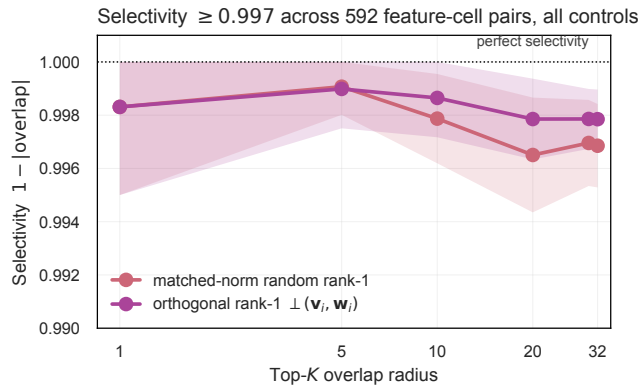


Figure 10: **Selectivity ≥ 0.997 across 592 feature-cell pairs at every measured K and every control.** Mean selectivity at Top- K overlap $K \in \{1, 5, 10, 20, 30, 32\}$ for matched-norm random rank-1 (red) and orthogonal rank-1 $\perp (\mathbf{v}_i, \mathbf{w}_i)$ (purple); flat-SVD coincides with random and is not drawn. Shaded bands 95% CI over $n=592$ (layer, head, feature) triples; no control dips below 0.996. Qwen3.5-0.8B L1/L9/L17.

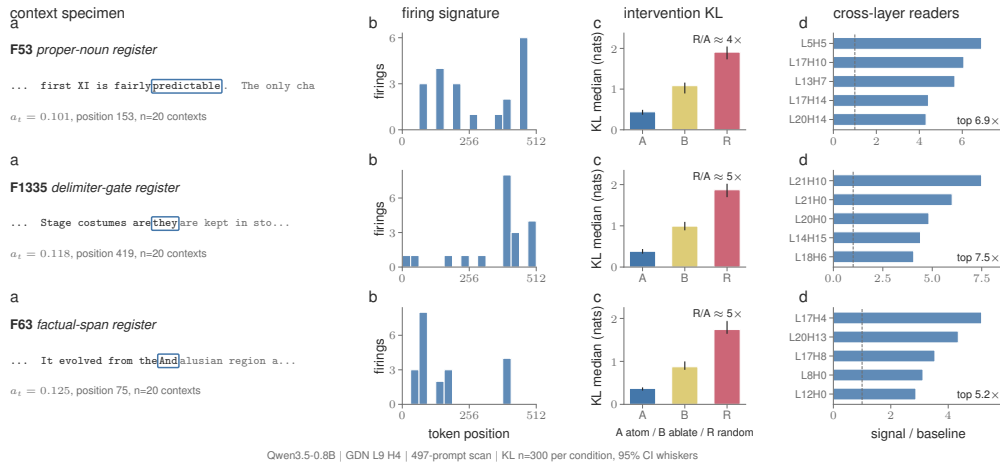


Figure 11: **Three register exemplars from Table 1 share write geometry and split surface roles.** Rows: F53 proper-noun register, F1335 delimiter gate, F63 factual-span register, all at Qwen3.5-0.8B GDN L9 H4. Columns: (a) one top-firing context with the firing token boxed, fire rate at left; (b) firing-rate histogram by token position over 497 prompts, showing position-distributed firings rather than a positional artefact; (c) median KL at the final output distribution under matched-Frobenius rank-1 substitution (A: SAE atom, B: deleted write, R: random rank-1), with 95% CI whiskers from $n=300$ per condition; (d) top cross-layer attention readers ranked by signal-to-baseline ratio. Atom substitutions remain near the deletion KL, while random controls increase KL by four to five times. Reader ratios in the 5.2–7.5 \times range identify specific late-layer heads that read each atom’s rank-1 write.

Table 9: **Per-experiment deviations from Table 8.** Only listed fields differ from the matched-cohort GDN configuration.

Experiment	Deviations from default
Encoder-swap ablation	SAE family $\in \{\text{flat, rank1, bilinear, bilinear_tied, bilinear_flat}\}$; matched optimizer/LR/batch/epochs/ k/n_{feat} .
Higher-rank decoder sweep	rank $\in \{1, 2, 4\}$ on bilinear; otherwise default.
BatchTopK family-invariance	use_batchtopk=True; same $k=32$.
JumpReLU family-invariance	sparsity rule = JumpReLU, $\lambda_{\text{sparsity}}=10^{-5}$, $\theta_0=10^{-4}$, bandwidth schedule cosine $10^{-3} \rightarrow 10^{-5}$, $L_0 \approx 1142$.
Gated SAE (negative)	three gate variants tested; all collapsed or destabilized.
k -vs-head curve	k swept $\in \{16, 32, 64\}$ at fixed $n_{\text{feat}}=2048$.
Per-firing KL test	no SAE training; uses matched-cohort checkpoints. Cache deep-copied per conditional forward.
Rank-1 perturbation propagation (Experiment C)	no SAE training; closed-form prediction via $\hat{\Delta} = \mathbf{v}_i^\top S_t \mathbf{w}_i \cdot W_{\text{out}} \text{vec}(\mathbf{v}_i \mathbf{w}_i^\top)$, $\varepsilon \in \{0.25, 0.5, 0.75, 1.0\}$, 500 prompts \times 50 features \times 4 scales \times 64 eval tokens, seed 2026.
Steering / 4B held-out probe	inference-time only; matched-cohort 0.8B checkpoints with bilinear matched-filter encoder.
Mamba-2 multi-head sweep	50 epochs, batch 128, warmup 100.

Table 10: **WriteSAE architecture variants.** ‘‘Bilinear’’ encoder $a_i = \mathbf{v}_i^\top S_t \mathbf{w}_i$; ‘‘Flat’’ encoder is dense linear on $\text{vec}(S_t)$. Dead-feature loss ($k_{\text{aux}}=256$, $\lambda_{\text{aux}}=10^{-2}$) and resampling cadence shared across rows.

Variants	Encoder	Decoder	Bias	Norm constraint
FlatSAE	dense linear on $\text{vec}(S_t)$	dense linear, $d_{\text{in}} \times n_{\text{feat}}$	none	decoder column unit-norm
MatrixSAE	dense linear on $\text{vec}(S_t)$	rank-1 outer product $\mathbf{v}_i \mathbf{w}_i^\top$	none	decoder factors unit-norm
BilinearSAE	matched filter $\mathbf{v}_i^\top S_t \mathbf{w}_i$	rank-1 outer product (untied factors)	none	encoder & decoder factors unit-norm
BilinearSAE (tied)	matched filter (tied to decoder)	rank-1 outer product (factors shared with encoder)	none	shared factors unit-norm
BilinearSAE (flat decoder)	matched filter	dense linear, $d_{\text{in}} \times n_{\text{feat}}$	none	decoder column unit-norm; encoder factors unit-norm

E Mechanism Support Figures

F Cross-Architecture Partition and Scaling

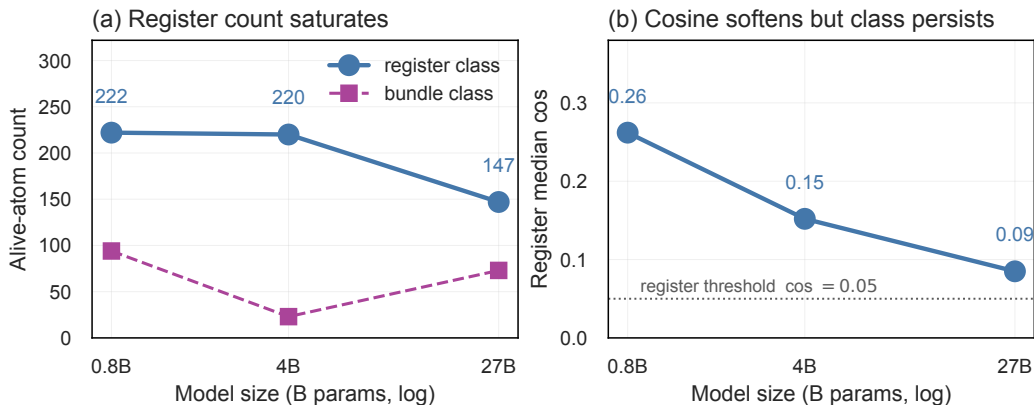


Figure 12: **Register class persists across the $34 \times$ Qwen3.5 scale range.** (a) Alive-atom counts at 0.8B / 4B / 27B. Register count stable near ~ 220 at 0.8B and 4B, 147 at 27B. (b) Register median cosine softens from 0.26 to 0.09 but never crosses the register threshold $\text{cos} = 0.05$. Qwen3.5-0.8B L9 H4 / 4B L12 H8 / 27B L32 H16.

F.1 All L9 heads

Re-run of the firing-level test on every L9 head (200 firings per feature, 400 prompts). The atom beats deletion on $89.29\% \pm 2.63\%$ of firings on average across 15 heads with firings (range 82.61–93.20%); L9 H4 is 90.84%, $+0.59\sigma$ above the mean. 14/15 heads exceed 85%, 12/15 exceed 88%. The main-text cell is representative of L9, not selected on the dependent variable.

Table 11: **The 11.7× DeltaNet-vs-Qwen27B gap (KS $p=1.2 \times 10^{-10}$) separates the tested host groups.** Outer-product-write cells have register/null ratios 60–383× with high dead counts; diagonal or scalar-gated cells show lower ratios (25–58×, dead 0–3). DeltaNet L12 H8 $k=128$ reaches $\cos=0.997$ at $n_{\text{reg}}=6$. Per-cell SAEs at $n_f=2048$.

Configuration	$n_{\text{reg}} / n_{\text{bun}}$	register median cos	ratio to null	dead
<i>Outer-product write</i>				
DeltaNet 1.3B L12 H8 $k=32$	0 / 118	–	–	1,930
DeltaNet 1.3B L12 H8 $k=64$	2 / 442	0.218	252×	1,604
DeltaNet 1.3B L12 H8 $k=128$	6 / 425	0.997	383×	1,617
DeltaNet 1.3B L6 H8 $k=64$	4 / 377	0.524	351×	1,667
DeltaNet 1.3B L18 H8 $k=64$	21 / 110	0.209	85×	1,917
Qwen3.5-0.8B L9 H4	222 / 94	0.262	192×	1,732
Qwen3.5-4B L12 H8	220 / 23	0.152	116×	1,805
Qwen3.5-27B L32 H16	147 / 73	0.085	60×	1,828
<i>Diagonal or scalar-gated write</i>				
Mamba-2 370M L24 H0 $k=64$	217 / 1,831	0.0575	58×	0
GLA 1.3B L12 H0 $k=64$	564 / 1,481	0.110	25×	3

Table 12: **Per-head replacement results at Qwen3.5-0.8B L9.** L9 register feature set [1442, 412, 192, 97, 1361, 53, 63, 87, 1335]. H12 has no firings.

Head	n_{records}	atom wins %	median KL_{atom}	median $\text{KL}_{\text{delete}}$
H0	1,000	91.90	1.07	1.90
H1	515	89.13	0.47	1.04
H2	177	85.31	0.42	0.96
H3	392	88.27	0.52	1.08
H4	1,277	90.84	0.41	1.09
H5	1,000	93.20	0.75	1.56
H6	427	88.52	0.39	0.88
H7	200	92.50	0.32	0.78
H8	601	87.35	0.37	0.87
H9	314	89.81	0.49	1.11
H10	23	82.61	0.23	0.54
H11	253	90.12	0.44	0.95
H12	–	–	–	–
H13	1,213	89.37	0.41	1.01
H14	697	90.10	0.36	0.84
H15	800	90.38	0.46	1.17
Mean (15 heads)	–	89.29 ± 2.63	–	–

F.2 Population-level 4-way KL test at L9 H4

Same protocol as Section 3.2 extended from the 8-feature example pool to the alive-atom population: 94 bundle atoms ($\overline{\cos} < 0.05$) plus 61 stratified register atoms, 155 total, capped at 30 firings per atom. 87 atoms reach the ≥ 5 -firing inclusion threshold.

Across 87 atoms, the atom beats deletion on **89.80%** of firings on average (95% CI [88.1, 91.3] over 2,426 firings; median 90.0%, range 60.9–100%). Class breakdown: 91.36% register ($n=30$), 88.98% bundle ($n=57$); Mann-Whitney $p=0.239$. Pearson $r=0.19$ between cosine and per-atom win rate ($p=0.08$); Spearman $\rho=0.06$ ($p=0.60$). Cosine to the native write tracks dictionary geometry; it does not predict substitution success at firing-level resolution.

Table 13: **The atom beats deletion on 89.80% of firings across 87 alive atoms (95% CI [88.1, 91.3]).** Win rates are near $\sim 90\%$ across cosine bins except [0.05, 0.20) where 10 atoms straddle the threshold.

Cosine bin	n_{atoms}	n_{firings}	atom wins %
$\cos < 0.00$	26	481	91.5
$0.00 \leq \cos < 0.05$	68	1,069	88.0
$0.05 \leq \cos < 0.20$	10	122	81.1
$0.20 \leq \cos < 0.30$	33	480	92.9
$\cos \geq 0.30$	18	274	92.7
All atoms (firing-level)	155	2,426	89.85
≥ 5 firings (per-atom mean)	87	2,426	89.80

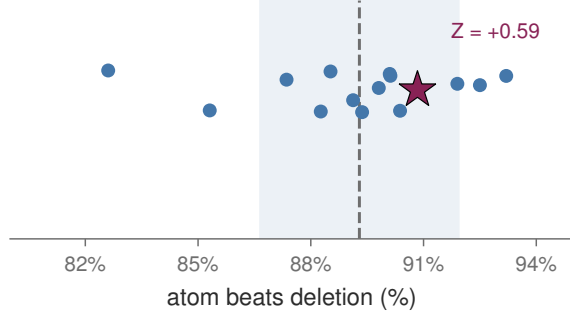


Figure 13: **L9 H4 lies within the bulk of the per-head distribution.** Win rate across all 15 L9 heads with firings (mean $89.29\% \pm 2.63\%$). Red star marks L9 H4 at 90.84%.

Table 14: **Per-head rank-1 vs rank-2 at Qwen3.5-0.8B L9.** Rank-2 lowers mean validation MSE by 3.1% and wins on 11/15 heads with both ranks trained, but the all-head substitution gives downstream perplexity 20.360 at rank-2 vs 20.347 at rank-1.

Head	MSE_{r_1}	MSE_{r_2}	MSE_{r_2}/MSE_{r_1}	n_{records}	atom wins %
H0	5.05×10^{-6}	4.92×10^{-6}	0.974	1,000	91.90
H1	3.04×10^{-6}	3.09×10^{-6}	1.017	515	89.13
H2	6.76×10^{-6}	6.53×10^{-6}	0.966	177	85.31
H3	3.00×10^{-6}	2.96×10^{-6}	0.985	392	88.27
H4	2.17×10^{-5}	2.17×10^{-5}	1.000	1,277	90.84
H5	1.01×10^{-6}	9.81×10^{-7}	0.972	1,000	93.20
H6	5.14×10^{-6}	5.10×10^{-6}	0.994	427	88.52
H7	1.38×10^{-5}	1.32×10^{-5}	0.950	200	92.50
H8	1.60×10^{-5}	1.57×10^{-5}	0.984	601	87.35
H9	6.84×10^{-6}	6.51×10^{-6}	0.952	314	89.81
H10	1.39×10^{-5}	1.21×10^{-5}	0.876	23	82.61
H11	5.21×10^{-7}	5.28×10^{-7}	1.014	253	90.12
H12	2.55×10^{-6}	2.99×10^{-6}	–	0	–
H13	–	5.36×10^{-6}	–	1,213	89.37
H14	1.99×10^{-6}	1.80×10^{-6}	0.905	697	90.10
H15	6.71×10^{-7}	6.77×10^{-7}	1.009	800	90.38
Mean (15 heads)	6.80×10^{-6}	6.59×10^{-6}	0.969	–	89.29 ± 2.63

F.3 Per-head rank-1 vs rank-2 reconstruction at L9

The rank-2 reduction does not propagate to substitution: rank-2 perplexity exceeds rank-1 by 0.013 nats. Gated DeltaNet writes one rank-1 outer per step, so a rank-2 atom decomposes into rank-1 atoms the dictionary already covers, or compresses an r -step write history the cache cannot accept at firing level.

F.4 Flat-SAE plus top-1 SVD substitution protocol

The cross-architecture baseline trains a flat TopK SAE on $\text{vec}(S_t)$ at the same cell as the architecture-matched WriteSAE, then reduces each firing’s reconstructed state to its leading SVD outer product. Flat dimensions: Gated DeltaNet 16,384 (128×128), Mamba-2-370M L24 H0 8,192 (128×64), RWKV-7-1.5B L12 H0 matched to per-head outer write. Training matches WriteSAE ($n_{\text{feat}}=2,048$, $k=32$, seed 42, 20 epochs, peak LR 3×10^{-4}). At evaluation we encode S_t , reshape into \hat{S}_t , take top-1 SVD outer $\hat{S}_t^{(1)} = \sigma_1 \mathbf{u}_1 \mathbf{v}_1^\top$, rescale to native Frobenius norm, and substitute. Per-firing replay caps firings per feature at three. Sample sizes: $n=1,851$ Gated DeltaNet, 2,367 Mamba-2, 6,591 RWKV-7. Source JSONs at `flat_sae_svd_{gdn,mamba2,rwkv7}`.

G Alternative Explanations Considered

Five readings could in principle reduce the partition to an artifact:

- **Decoder rank-1 prior:** App. C shows encoder-swap MSE within 8% of the dense flat upper bound at L1/L9.
- **Exemplar selection:** App. G.2 cosine-free classifier replicates the main substitution result.
- **Threshold fragility:** 92.4% ordering holds within $\pm 2\text{pp}$ across $0.5 \times -2 \times$ threshold sweeps, 10^4 -sample permutation $p < 10^{-4}$, replicating at L1 H4 + L17 H4 on $n=4,851$ events.

- **Small-model artifact:** Qwen3.5-4B L12 H8 reproduces the partition at $116\times$ register/null ratio, 27B L32 H16 at $60\times$ (Section 6.1, App. F).
- **Random failure distribution:** Fig. 14 shows the 7.6% cases where deletion beats the atom concentrate on smallest-effect-size firings (Q1 12.3% vs Q4 4.9%), consistent with the smallest effects being hardest to distinguish.

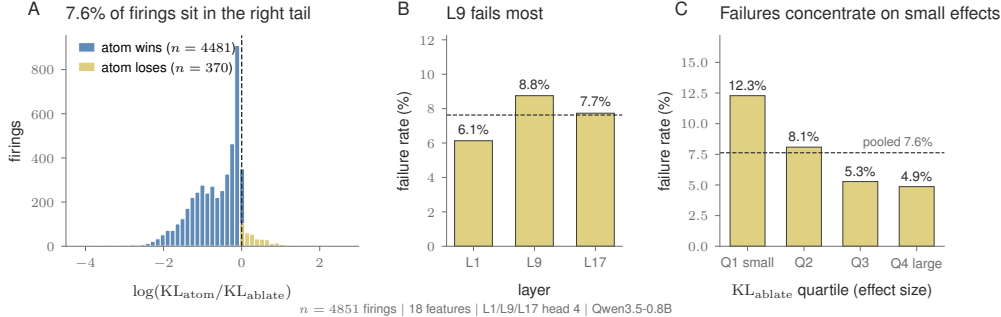


Figure 14: **Deletion beats the atom mainly on small-effect firings.** (a) $\log KL_{\text{atom}}/KL_{\text{delete}}$ over $n=4,851$ firings (L1/L9/L17, 0.8B): 4,481 atom wins, 370 losses (7.6%). (b) Per-layer failure rate close to the 7.6% pooled mean. (c) Failure rate by KL_{delete} effect-size quartile: Q1 12.3% to Q4 4.9%.

G.1 Cosine threshold and mixture order

Sweeping τ and the GMM mixture order at L9 H4 does not change how often the atom beats deletion. The 0.8B count moves $1.10\times$ across $\tau \in \{0.02, 0.03, 0.05, 0.10\}$; at every τ the replacement win rate remains in the 90–94% band. GMM $k=3$ adds a third component at weight 0.175 but $\Delta\text{BIC}(k=2 \rightarrow k=3)=-4.15$ favors the two-component fit (bimodality coefficient 0.208, threshold not reached). The k -sweep at L9 H4 runs 67/100/1,881 register/bundle/null at $k=16$, 76/97/1,875 at $k=32$, 155/137/1,756 at $k=64$.

Table 15: **Partition counts shift but replacement remains stable across τ and k .** Per-class win rate at L9 H4 is 91.25% on the register pool chosen by replacement success and stays in $[90.7, 94.0]\%$ across the cosine partition’s two classes.

Cosine threshold τ	0.02	0.03	0.05	0.10
Qwen3.5-0.8B L9 H4 register count	243	235	222	221
Qwen3.5-0.8B L9 H4 bundle count	73	81	94	95
Qwen3.5-4B L12 H8 register count	227	224	220	183
Qwen3.5-4B L12 H8 bundle count	16	19	23	60
GMM mixture order k	$k=2$		$k=3$	
BIC at L9 H4	−679.18 (preferred)		−683.33 ($\Delta=-4.15$)	
k -sweep ($n_f=2,048$)	$k=16$	$k=32$	$k=64$	
L9 H4 register / bundle / null	67/100/1,881	76/97/1,875	155/137/1,756	

G.2 Cosine-free classifier reproduces the substitution result

F758 demotion. F758 has the highest single-atom cosine (0.985) but fires at 5×10^{-4} activation rate; its few hits came from an amplified scan at $5\times$ mean register activation. F1335 is the main-text exemplar because it fires on 5.24% of validation tokens.

A replacement-success classifier on the L9 H4 feature pool that reads no decoder geometry (register if the atom beats deletion on more than half its firings, bundle otherwise) agrees with the cosine-classifier on 7 of 8 features that fired above threshold. The single disagreement is F87, the canonical bundle exemplar at $\widehat{\text{cos}}=0.012$, whose atom beats deletion on 94% of its 300 firings. The logit formula explains why two coordinates disagree at a single atom while agreeing at the class level.

The cosine-free pool reproduces the main result. The replacement-success register class fires 1,851 times, with the atom beating deletion on 91.25% of firings, the same number reported in Section 3.2. Cosine-register fires 1,551 times at 90.72%; cosine-bundle is F87 alone at 94.00%. The two classes report the same per-firing rate within 3pp; removing cosine from the pipeline leaves the 91% result unchanged. The 8-feature pool was selected register-skewed (Cohen’s κ degenerates), so the relevant evidence is the per-class win rate. App. F.2 extends to 87 atoms: 88.98% on cosine-bundle ($n=94$), 91.36% on cosine-register ($n=61$), Mann-Whitney $p=0.239$.

Table 16: Class-level claims replicate across SAE seeds; per-atom identity does not.

Claim	Granularity	Evidence
Register/bundle partition	Class-level	GMM $\Delta\text{BIC} = -296$; CV 4–12% across 3 seeds
Partition scale-invariance	Class-level	$34\times$ Qwen range; DeltaNet sweep
Register firings direction-selective	Class-level	Selectivity 0.9953 across 47/48 cells
Atom beats deleting the write	Firing-level	92.4% of $n=4,851$; permutation $p < 10^{-4}$, Cliff’s $\delta = +0.825$. Population on 87 atoms: 89.80%, CI [88.1, 91.3]
Individual atom identity (e.g., F758)	Per-atom	$< 1\%$ basis overlap across seeds (illustrative)

G.3 DeltaNet substitution failure: geometric and causal decoupling

DeltaNet L12 H8 produces the largest register-cosine separation (register median $\cos = 0.997$, register/null $383\times$ at $k=128$; Tab. 11), yet the firing-level substitution test on the same cell fails. On $n=395$ firings across 37 passages, the strict ordering $\text{KL}_{\text{atom}} < \text{KL}_{\text{delete}} < \text{KL}_{\text{random}}$ holds on 17.7% of firings (CI [14.0, 21.5]), against 89.5% on the Qwen3.5-0.8B L9 H4 Gated DeltaNet cell. The atom beats deletion on 48.3% of firings, indistinguishable from chance. Median $\text{KL}_{\text{atom}} = 2.70 \times 10^{-4}$ exceeds median $\text{KL}_{\text{delete}} = 2.30 \times 10^{-4}$.

DeltaNet runs the bilinear write rule with the convex gate off (`use_gate=false`), so S_t accumulates without per-position decay. Top-1 singular variance is 97.79% (stable rank 1.023), so the state is geometrically rank-1, but the dominant singular direction integrates every prior write. The atom matches the average direction of $\mathbf{k}_t \mathbf{v}_t^\top$ across positions; under no decay, the cache at firing time is set by integrated history, not the local write the atom is trained to recover. Adding a gate (Qwen3.5 Gated DeltaNet) restores per-position decay and the replacement test recovers (Tab. 11, atom beats deletion on $> 89\%$ throughout the $34\times$ Qwen range).

H Register vs bundle: systematic differences beyond population win rate

The population test in App. F.2 reports a null gap in how often the atom beats deleting the write (91.4% vs 89.0%, $p=0.24$). Beyond binary win/loss, the two classes differ on quantities that affect interpretive use of the partition. We re-use the 87 alive atoms from the L9 H4 population KL run; 23 register and 56 bundle atoms enter the top-1 analyses, with 2,190 records carrying per-firing top-1 token id, next-token rank, and log-probability under each cache state.

Table 17: Register and bundle classes differ on three of four causal axes at L9 H4. Top-1 disrupt is the fraction of firings on which the patched cache flips the model’s top-1 next-token. ΔKL is per-atom median $\text{KL}_{\text{delete}} - \text{KL}_{\text{atom}}$ (nats). Firings per atom is the activation count over 10,000 validation tokens. Cliff’s δ positive: register $>$ bundle. Mann-Whitney p two-sided.

Axis	Register median	Bundle median	Cliff’s δ	MW p
ΔKL (nats)	0.682	0.579	+0.109	0.45
Top-1 disrupt under deletion	0.700	0.633	+0.294	0.041
Top-1 disrupt under atom	0.423	0.400	+0.161	0.26
Firings per atom (population scan)	100	70.5	+0.518	$< 10^{-3}$

Top-1 disruption. Removing a register flips the top-1 on 70.0% of firings, against 63.3% for a bundle (Cliff’s $\delta = +0.29$, $p=0.041$); cosine vs deletion top-1 flip-rate Pearson $r = +0.25$ ($p=0.027$). The atom-state top-1 disrupt is statistically tied across classes, so the rank-1 atom recovers the native top-1 at comparable rates whether the underlying write is cosine-aligned or not.

Firing breadth. Registers fire on a median of 100 validation tokens; bundles on 70.5 ($\delta = +0.52$, $p < 10^{-3}$). Cosine-vs-firing-count Spearman $\rho = +0.73$ ($p < 10^{-5}$) is the strongest continuous correlation in this analysis. The interpretive consequence: register atoms supply more firing examples per unit of validation traffic, making them cheaper to recruit for circuit-tracing or edit experiments.

ΔKL effect size. Median ΔKL is 0.682 nats for registers and 0.579 for bundles (Cliff’s $\delta = +0.11$, $p=0.45$). The two classes inflict comparable lesion magnitude, consistent with the null on win rate.

Behavioral wedge beyond F87. The cosine-free flip of F87 (App. G.2, atom beats deletion on 94% of firings) is one point on the continuous gradient above. The cosine partition predicts which atoms carry more next-token mass and how often they fire, even though it does not predict whether a given firing’s substitution beats deleting the write; the firing-level test holds across the full alive dictionary at 89.8%.

I Extended Results: Selectivity, Reader Traces, and Residual-SAE Comparison

I.1 Selectivity sanity check and orthogonal-rank-1 control

An orthogonal rank-1 control at matched Frobenius norm returns selectivity 0.998; any matched-norm rank-1 perturbation, aligned or orthogonal, scores above 0.99, so top- K -overlap selectivity cannot separate the SAE atom from a random rank-1 (Fig. 10). Top- K -overlap selectivity averages **0.9953** across 47/48 cells under matched-norm random rank-1 perturbation (CI [0.9930, 0.9976]). The distinguishing evidence is firing-level KL ordering, the population substitution test (App. F.2), and the amplitude-conditional F87 inversion.

I.2 Reader traces at L9 H4 exemplars

Register atoms read into specific later attention heads at 3–7 \times baseline (F53 into L5 H5 at 6.9 \times , F63 into L17 H4 at 5.2 \times , F1335 into L21 H10 at 7.5 \times); the signal does not diffuse across the residual stream. These three exemplars show reader-enriched pathways, but we do not claim generality.

I.3 Residual-stream SAE on the same model

A residual-stream SAE asks a different question: its cosine measures alignment between an atom and the activation the dictionary was trained to reconstruct, an alignment the TopK objective guarantees [Gao et al., 2025, Sun et al., 2025]. On Qwen3.5-0.8B, a TopK SAE on the L15 attention output ($n_{\text{feat}}=2,048$, $k=32$) returns 1,848 register atoms against 27 bundles at register median $\cos=0.21$ ($\Delta\text{BIC}=+306.5$), against 222 and 94 on the GDN cache. The substitution test instead measures cosine to $\mathbf{k}_t \mathbf{v}_t^\top$, an object the dictionary was not trained against. Residual-stream atoms are vectors; they cannot occupy the cache slot the rank-1 atom replaces.

I.4 Memory-edit intervention

The cache edit reported in Section 4 runs at L9 H4 on the same dictionary used for the firing-level KL ordering. Records are at `jackyoung27/writesae-ckpts/results/memory_edit_F412/` as `summary.json`, `records.jsonl`, `dose_response.csv`, `feature_detection.json`.

Feature detection. For each F412 firing we sum $\log p_{\text{native}} - \log p_{\text{delete}}$ across firings per token id; the highest-scoring token is the feature’s preferred token. F412’s winner is Qwen tokenizer id 98818 (gloss “space”), summed native-minus-delete difference 14.5 nats. Median natural activation $a^*=0.31$.

Erasure at natural firings. At $n=150$ natural firing positions, deleting the write changes the preferred token’s log probability by median -0.116 nats, 95% CI $[-0.265, -0.042]$, paired Wilcoxon $p=1.07 \times 10^{-6}$, mean -0.349 . Preferred-token rank shifts from native median 68,485 to patched median 77,444.

Table 18: **Erasure at $n=150$ natural firings of F412 (Qwen3.5-0.8B L9 H4) reduces the atom’s preferred next-token probability.** Preferred token: Qwen id 98818 (“space”).

Quantity	Value
n firings	150
Median $\Delta \log p$ (preferred token)	-0.116 nats
95% CI	$[-0.265, -0.042]$
Mean $\Delta \log p$	-0.349 nats
Paired Wilcoxon p	1.07×10^{-6}
Native median rank (preferred token)	68,485
Patched median rank (preferred token)	77,444

Cache edit at non-firing positions. At $n=150$ non-firing positions we add $m \cdot a^* \cdot \mathbf{v}_{F412} \mathbf{W}_{F412}^\top$ to the cache. No tested magnitude reaches significance; per-position writes at non-firing slots are dominated by surrounding context. Dose-response over $n=50 \times 6$ magnitudes returns a weakly monotone trend with no significant linear fit.

Table 19: **Cache edits at $n=150$ non-firing positions do not reach significance.**

Magnitude	Median $\Delta \log p$	p
$1 \times a^*$	$+3.1 \times 10^{-5}$	0.67
$2 \times a^*$	+0.008	0.28
$4 \times a^*$	+0.016	0.15

I.5 Single-position sign test

For each target token T we compute $v_T^* = W_O[\text{head}]^\top W_U[T]/\|\cdot\|$, write that direction at one cache position, and measure the target token’s logit change. Pooled run $n=2,000$ triples at L9 H4: pooled $R^2 = -0.06$ (measured scale varies with prompt context), directional agreement 84.6% CI [83.0, 86.2], Pearson $r=0.162$ ($p=3.7 \times 10^{-13}$), median measured/predicted ratio 1.08.

I.6 Generation intervention: full results

The direction $v_T^* = W_O[\text{head}]^\top W_U[T]/\|\cdot\|$ is chosen to increase the logit of target token T under a rank-1 cache write. Sweep: 30 prompts \times 5 cache positions \times 8 targets \times 3 magnitudes = 3,600 trials at L9 H4. Each edit is applied across three consecutive cache positions at $m \cdot \|\mathbf{k}_t \mathbf{v}_t^\top\|$; the model then generates 20 tokens greedily. Targets are stratified by their initial rank under the unmodified model: *frequent* ($\sim 17,000$), *rank 100–1000*, *rare* ($\geq 10,000$), and *semantic* (out-of-context).

Table 20: **Pooled target-appearance lift by magnitude across $n=1,200$ trials per row.** Lift subtracts the unmodified model’s rate (8.3%). $3\times$ gives the largest measured lift.

Magnitude	target appears after edit	lift (pp)	rank improved	median logp lift (nats)
1.5 \times	16.7%	+8.3pp	—	—
3.0 \times	25.0%	+16.7pp	77.4%	+1.27
6.0 \times	16.7%	+8.3pp	—	—

Table 21: **Breakdown by target class at $m=3\times$ ($n=300$ per class).** Targets initially ranked 100–1000 reach 100% vs 33.3% under the unmodified model (+66.7pp). Out-of-context classes show 4,039–17,526-position rank shifts but 0% target appearance because greedy generation cannot promote a starting rank $\geq 17,000$ to top-1 over three positions.

Class	initial rank	edited	native	lift (pp)	median rank shift
frequent (out-of-context)	$\sim 17,000$	0%	0%	0	17,526
rank 100–1000	100–1000	100%	33.3%	+66.7	517
rare	$\geq 10,000$	0%	0%	0	16,800
semantic (out-of-context)	—	0%	0%	0	4,039

Rank 100–1000 result. For targets initially ranked 100–1000 under greedy decoding, the $m=3\times$ cache edit yields 300/300 continuations with the targeted token. Pooled across all four classes the lift is +16.7pp (25.0% vs 8.3% native, $n=1,200$); restricted to the rank-100-to-1000 class, the lift is +66.7pp.

Stratification note. The frequent, rare, and semantic classes were drawn from out-of-context vocabulary items that the unmodified model ranks at least 17,000. They produce 0% target appearance at every magnitude. The direction chosen by the formula shifts these tokens by 4,039–17,526 rank positions; the underlying logit signal appears, but greedy decoding over three cache positions cannot move the starting rank to top-1. The rank-100-to-1000 class meets both conditions; out-of-context classes meet only the first.

Magnitude saturation. Pooled lift is non-monotone: +8.3pp at 1.5 \times , +16.7pp at 3.0 \times , +8.3pp at 6.0 \times . Beyond the best measured magnitude, the cache write dominates surrounding context and degrades the rest of generation, mirroring the newline-rate saturation at 10 \times in Section 4.

J Reproducibility

Code, checkpoints, license. All scripts that produce the reported numbers, tables, and figures are in the repo snapshot at <https://github.com/JackYoung27/writesae>. Trained SAE checkpoints, cached Gated DeltaNet state tensors, and per-head deletion-control JSON outputs are on HuggingFace at [jackyoung27/writesae-ckpts](https://huggingface.co/jackyoung27/writesae-ckpts) (four SAE variants \times Qwen3.5-0.8B/4B/27B; 0.8B covers L9 and L1 H4, L17 H4). Code and checkpoints under MIT; base models under Tongyi Qianwen. ~ 180 H100-hours single-GPU; one canonical SAE config fits in ~ 6 H100-hours. Reference container `pytorch/pytorch:2.4.1-cuda12.1-cudnn9-runtime` with pinned transformers, `flash-linear-attention` [Yang and Zhang, 2024], `datasets`, `h5py`, `huggingface_hub`; `pip install -e .` reproduces outside the container.

Datasets. OpenWebText [Gokaslan and Cohen, 2019] streamed from `SkyLion007/openwebtext` (CC0). Tokenize with the Qwen3.5 tokenizer (152K BPE, shared across 0.8B/4B/27B), pack into 1,024-token blocks. Gated DeltaNet on $5,000 \times 1,024$ sequences yields $\approx 5 \times 10^6$ matrix-valued samples per head, 80/20 train/val at seed 42. Evaluation pulls disjoint shards: 500 sequences for the cache-replacement PPL sweep (positions 0–511 context, teacher-forced loss on 512–1023) and 20 paired-connector passages for the bits/token comparison (Fig. 2b). The 4B generation probe uses a third 40-prompt set, disjoint from training, PPL, and connector splits.

Per-firing atom selection. The firing-level substitution test in Section 3.2 uses the dominant atom of the SAE’s TopK encoding at each firing position:

```

for each firing position t of feature i:
  a  = SAE.encode(S_t)                # k = 32 nonzeros
  j  = argmax_{r in TopK(a)} a_r      # dominant atom
  A_j = decoder_v[j] @ decoder_w[j].T # rank-1 outer
  sigma_t = norm(beta_t * k_t @ v_t.T, 'fro') / norm(A_j, 'fro')
  write_substitute = sigma_t * A_j    # matched norm
  forward(state := previous + write_substitute) # atom/delete/random

```

The deletion condition writes a zero outer product at matched Frobenius norm; the random rank-1 condition draws from the matched-norm random routine. Gated DeltaNet mutates its cache in place, so per-firing replay deep-copies the cache for each conditional forward pass.

Implementation notes. Alive-feature counts on the dense-encoder WriteSAE stay in the 300–1,200 range only with both regularizers: an auxiliary dead-feature loss ($\lambda_{\text{aux}}=10^{-2}$) reconstructs residuals through atoms silent for 100 steps, and a resampler fires every 250 steps for atoms still silent after the auxiliary term. Dropping either roughly doubles the dead-atom rate. The dense encoder reaches the lowest validation MSE on every cell tested but its atoms do not carry a clean rank-1 read; the bilinear matched-filter encoder $a_i = \mathbf{v}_i^T S_t \mathbf{w}_i$ trails MSE by 5–15% but its firing coefficient matches the state’s projection onto the same rank-1 direction the decoder writes, so we use it for the 4B generation probe. Skipping the cache deep-copy biases results toward whichever condition runs last (cost $\sim 1.4\times$ wall-clock per firing).